Holocene warming and evergreen/deciduous forest replacement across eastern China

Zhuo Zheng, Cong Chen, Kangyou Huang, Xiao Zhang, Peter Kershaw, Jun Cheng, Jie Li, Yuanfu Yue, Qiuchi Wan, Yaze Zhang, et al.

▶ **To cite this version:**

Zhuo Zheng, Cong Chen, Kangyou Huang, Xiao Zhang, Peter Kershaw, et al.. Holocene warming and evergreen/deciduous forest replacement across eastern China. Quaternary Science Reviews, 2023, 307, pp.108057. 10.1016/j.quascirev.2023.108057 . hal-04249127

HAL Id: hal-04249127
https://hal.science/hal-04249127

Submitted on 20 Oct 2023

HAL is a multi-disciplinary open access archive for the deposit and dissemination of scientific research documents, whether they are published or not. The documents may come from teaching and research institutions in France or abroad, or from public or private research centers.

L'archive ouverte pluridisciplinaire **HAL**, est destinée au dépôt et à la diffusion de documents scientifiques de niveau recherche, publiés ou non, émanant des établissements d'enseignement et de recherche français ou étrangers, des laboratoires publics ou privés.

Holocene warming and evergreen/deciduous forest replacement across eastern China

Zhuo Zheng[a,b*†], Cong Chen[a†], Kangyou Huang[a,b*], Xiao Zhang[a], Peter Kershaw[c], Jun Cheng[d], Jie Li[e], Yuanfu Yue[f], Qiuchi Wan[a], Yaze Zhang[a], Yongjie Tang[a], Mengyuan Wang[g], Xiayun Xiao[h], Rachid Cheddadi[i],

[a] *Guangdong Key Lab of Geodynamics and Geohazards, School of Earth Sciences and Engineering, Sun Yat-sen University, Zhuhai 519082, China*

[b] *Southern Marine Science and Engineering Guangdong Laboratory (Zhuhai), Zhuhai 519082, China*

[c] *School of Earth, Atmosphere and Environment, Monash University, Melbourne, VIC, 3800, Australia*

[d] *Key Laboratory of Meteorological Disaster, Ministry of Education (KLME)/Joint International Research Laboratory of Climate and Environment Change (ILCEC)/Collaborative Innovation Center on Forecast and Evaluation of Meteorological Disasters (CIC-FEMD), Nanjing University of Information Science and Technology, Nanjing 210044, China*

[e] *Qingdao Institute of Marine Geology, China Geological Survey, Qingdao 266071, China*

[f] *Guangxi Laboratory on the Study of Coral Reef in the South China Sea, Coral Reef Research Center of China, School of Marine Sciences, Guangxi University, Nanning 530004, China*

[g] *School of Marine Sciences, Sun Yat-sen University, Zhuhai 519082, China*

[h] *State Key Laboratory of Lake Science and Environment, Nanjing Institute of Geography and Limnology, Chinese Academy of Sciences, Nanjing 210008, China*

[i] *ISEM, University of Montpellier, CNRS, IRD, EPHE, France*

[†] *These authors contributed equally to this work: Zhuo Zheng and Cong Chen.*

e-mail (corresponding authors):

eeszzhuo@mail.sysu.edu.cn; hkangy@mail.sysu.edu.cn

ABSTRACT

Combined variations of insolation and ice sheet led to major global climatic and ecosystem changes between the Last Glacial Maximum (LGM) and the Holocene. However, little is known about effects of these changes on the alternating dominance of deciduous and evergreen vegetation in East Asia, particularly in the regions now dominated by evergreen broadleaved forest (EBLF) that forms a vast ecotonal zone between tropical and temperate belts. In this study, we have used two representative records in center of the EBLF distribution, associated with broader regional pollen data from eastern China, to reconstruct spatiotemporal biome changes over the last 22 ka. The results showed a dominance of deciduous broadleaved forest at the LGM in most mountainous regions of the subtropical zone, and the EBLF began to migrate and expand into the low latitude subtropical areas during the last deglaciation, particularly at ca.11.3 ka after the Younger Dryas. However, major biome replacement from deciduous to evergreen forest across eastern China did not occur until 8.1 ka, indicating an earlier forest replacement at sites in low latitude regions as compared to sites located further north or at higher mountains. Our evidence agrees well with quantitative climate reconstruction and simulations at local and regional scales, showing that forest transformed when thermal conditions reached relevant thresholds. Both simulated and reconstructed paleotemperatures are consistent with the early-to-middle Holocene being a key period when climatic thresholds (particularly winter and/or annual temperatures) gradually approached then exceeded bioclimatic constraints on EBLF recolonization. By contrast, the precipitation in most part of mountainous subtropical southeast China may not be a key constraint for evergreen/deciduous forest transformation since the last deglaciation. During the late Holocene, the reconstructed biome has shifted unstably, probably due to interactive effects of several regional-scale factors, including seasonal climate biases and major fluctuations in effective

moisture associated with weakening of summer monsoon before the enhanced human interventions of the last 3000 years.

Keywords: Evergreen broadleaved forest; Deglaciation; Holocene; Biome change; Transient simulation; Climate threshold.

1. Introduction

In East Asia, evergreen broadleaved forest (EBLF), also known as laurophyllous forest, is currently the most widespread vegetation type in the subtropical zone, extending from ~22° N, near the Tropic of Cancer, to the Yangtze River basin at 31-33° N in China and 33-35° N in southern Japan (Wu, 1980; Fang et al., 2011). During the Last Glacial Maximum (LGM), the mean surface temperature of mainland China and adjacent areas is estimated to have been 2-8°C colder than today (Jiang et al., 2011; Tian and Jiang, 2016). Simulated and reconstructed biome distribution patterns during the LGM indicate a large-scale southward shift of temperate deciduous forests (DBLF) in regions where EBLF dominates today, followed by a gradual recolonization by continental evergreen biomes during postglacial global warming (Yu et al., 2000; Kageyama et al., 2012; Ni et al., 2014). However, little is known about the high-resolution temporal changes in forest transformation from deciduous to evergreen vegetation and the threshold climatic conditions required for forest replacement across the Asia since the last deglaciation. Important questions remain regarding the timing of the onset, dynamics, and causes of this large biome transformation over the subtropical belt in East Asia (Zhao et al., 2009; Li et al., 2019).

As yet, there are few well-dated, high-resolution fossil records dating back to the LGM from subtropical regions (Zheng et al., 2016), which severely hinders reconstruction of the nature of spatial vegetation shifts and their relationships with past climate change. Moreover, the modeled cold-tolerant DBLF biome in southern China is poorly represented as a vegetation type in the LGM fossil pollen record, casting doubt on the accuracy of reconstructed vegetation, both spatially and temporally (Yu et al., 2000; Harrison et al., 2001). Therefore, we here have used two representative pollen records, together with other regional pollen and biomarker data, to reconstruct past biome changes, focusing on the EBLF's migration history in subtropical Asia. The two high-resolution records are located in a sensitive montane forest zone in central subtropical regions, where current climatic conditions are near the temperature thresholds for shifts between evergreen and deciduous forest. As temperatures constrain plant photosynthetic efficiency physiologically (Bai et al., 2010; Song et al., 2016), and thus are key controls of biome change between EBLF and DBLF, we quantitatively reconstructed paleotemperatures using pollen and biomarker data and linked them to local and regional climate simulations by a transient model. The results indicate dramatic biome and climate changes during the last 22 ka in subtropical Asia, and past temperature thresholds for forest transformation under deglacial warming from the LGM to the Holocene. The study has important implications for the projection of future forest migration in Asia under global warming.

2. Materials and Methods

2.1. Regional setting and materials

Vegetation in the subtropical zone of China is composed mainly of EBLF that can be divided into two main components: humid forest in southeastern China and semi-humid mountainous forest in southwestern China, the southeast margin of the Tibetan Plateau (Wu, 1980). The eastern subtropical humid EBLF region generally includes three subzones: a northern subtropical evergreen and deciduous broadleaved forest zone (STa), middle subtropical zone (STb) and southern subtropical zone (STc). The northern boundary of the subtropical zone is near a geographical line joining Qinling mountain ranges and Huaihe River, and the northern subzone (STa) is dominated by deciduous oak forest mixed with evergreen broadleaved trees. The STa subzone has also been assigned to an independent vegetation ecotone (evergreen-deciduous broadleaved forest) of the warm-temperate zone, dominated by deciduous trees (Fang et al., 2002). However, the large lowland river plains of this subzone are cultivated with rice and aquatic plants. The middle subzone (STb), restricted to the area between the Yangtze River and Nanling mountain ranges, is characteristically covered by EBLF dominated by evergreen genera such as *Cyclobalanopsis*, *Castanopsis*, *Lithocarpus*, *Schima*, *Machilus*, *Phoebe*, *Altingia*, *Elaeocarpus* and *Eurya*. The southern subzone (STc) hosts monsoonal humid evergreen forest characterized by genera from families including Fagaceae, Lauraceae, Theaceae, Myrtaceae, Meliaceae, Moraceae, Myrsinaceae, Rubiaceae and Hamamelidaceae. In the west, there is a semi-humid subzone (STw), typically comprising alpine EBLF characterized by montane sclerophilous *Quercus* (Sect. *Heterobalanus*), subalpine *Cyclobalanopsis* and pine forests (Wu, 1980). The distribution of EBLF in the subtropical East Asia is strongly influenced by monsoon climate circulation. The mean annual temperature of the EBLF distribution area is usually between 16 and 22°C, with a relatively warm winter generally higher than

0°C (Song, 1999). Annual precipitation generally exceeds 1100 mm (Fang and Yoda, 1991), and the relative humidity is about 75-80% on average.

We reconstructed past vegetation changes during the transition from the LGM, at around 22 ka, to the Holocene. For this, we used two high-resolution pollen records, based on cores from the sites of Gutian (GT) and Shuizhuyang (SZY) in the middle subtropical EBLF subzone (STb), together with other pollen data from sites across the zone (Fig. 1a, Table 1). The GT site is in the hinterland of the Yuecheng Mountains in the west Nanling Ranges, southern China (110.366°E, 26.084°N; 1677 m asl). This is in the southern part of the central subtropical zone, which is strongly influenced by the monsoon climate system. The local mean annual temperature is about 14-15°C, and the coldest mean temperature (January) is only 1-2°C at an altitude of about 1000 m. The annual precipitation, of 1200-1600 mm, is concentrated between the end of March and July. Lithologically, the GT core comprises a thin sand layer interbedded with gravel at the base, grey silty clay at 140-194 cm depth, dark clay with a high plant debris content at 22-140 cm, and brown root-rich gyttja in the upper 0-22 cm layer. The SZY core was collected from a mountain peat bog in Jiufeng Mountains, southeastern China (119.034°E, 26.777°N; 1007 m asl) (Yue et al., 2012). The site is in the mid-subtropical zone, with an annual mean temperature and precipitation of about 15°C and 1400-1800 mm, respectively. Zonal vegetation types at the GT and SZY sites are evergreen broadleaved and evergreen/deciduous mixed forest, respectively. Each site is in a summit wetland of a mountainous area, with a local landscape mainly covered by shrubs and grasses of various families, including Ericaceae, Theaceae, Saxifragaceae, Clethraceae, Rosaceae, Symplocaceae, Poaceae, Cyperaceae, and Asteraceae.

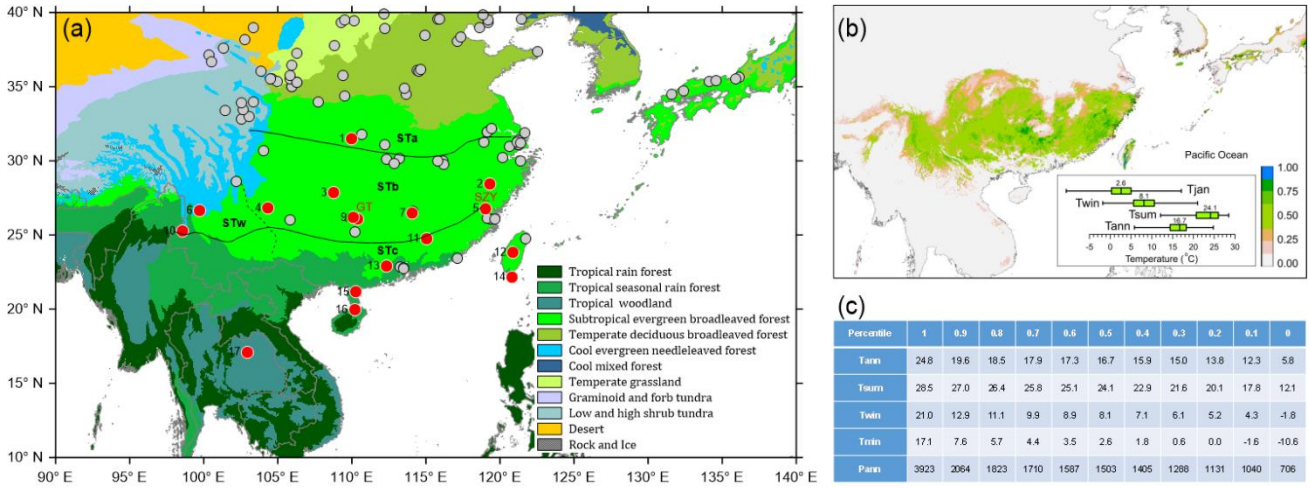

(c)

Percentile	1	0.9	0.8	0.7	0.6	0.5	0.4	0.3	0.2	0.1	0
Tann	24.8	19.6	18.5	17.9	17.3	16.7	15.9	15.0	13.8	12.3	5.8
Tsum	28.5	27.0	26.4	25.8	25.1	24.1	22.9	21.6	20.1	17.8	12.1
Twin	21.0	12.9	11.1	9.9	8.9	8.1	7.1	6.1	5.2	4.3	-1.8
Tmin	17.1	7.6	5.7	4.4	3.5	2.6	1.8	0.6	0.0	-1.6	-10.6
Pann	3923	2064	1823	1710	1587	1503	1405	1288	1131	1040	706

Fig. 1. Locations of the examined pollen records across East Asia, present-day biome map and simulated EBLF distribution. (**a**) Vegetation map showing the modern biomes in eastern Asia, in which the subtropical evergreen broadleaved forest (EBLF) zone is divided into northern (STa), middle (STb), southern (STc) and western (STw) subzones (Wu, 1980). The dots are locations of the examined pollen records from eastern China (108 sites in total), and those in red (1-17) were used for EBLF data integrations (Table 1). (**b**) The potential distribution of EBLF today as simulated by the Species Distribution Model (SDM). The most important bioclimatic thresholds are indicated using quartile values (25%, 50% and 75% in green boxes). (**c**) Percentiles for the five key climatic variables characterizing the EBLF distribution in southern China, based on 500 random grids of digital georeferenced data: annual precipitation (Pann) and mean temperatures of the coldest month (Tjan), winter (Twin), summer (Tsum), and year (Tann).

Table 1. Locations of 14 subtropical (1-14) and 3 tropical pollen records (15-17) for the regional EBLF integration study, selected from 108 examined sites across East Asia.

No.	Core (site name)	Location	Elevation (m)	Type of archive* and age range (ka BP)	Reference
1	DJH (Dajiuhu)	110.001°E, 31.484°N	1751	P (0-42)	Li et al., 2013
2	LTY (Lantianyan)	119.310°E, 28.430°N	902	L (1-8)	Ma et al., 2016
3	JLC (Fanjingshan)	108.775°E, 27.847°N	2200	P (0-10)	Gao et al., 2019
4	NT (Nantun)	104.340°E, 26.810°N	2203	L (1-22)	This paper

5	SZY (Shuizhuyang)	119.034°E, 26.777°N	1007	P (0-50)	This paper
6	TCK1 (Tengchong)	99.716°E, 26.641°N	3898	L (0-22)	Xiao et al., 2014
7	JXA (Jiangxi'ao)	114.092°E, 26.470°N	1650	P (0-11)	This paper
8	GT (Gutian)	110.366°E, 26.084°N	1677	P (0-21)	This paper
9	DP (Daping)	110.117°E, 26.167°N	1620	P (0-15)	Zhong et al., 2015
10	TCQH (Tengchong)	98.553°E, 25.261°N	1885	L (0-18)	Zhang et al., 2020
11	DH (Dahu)	115.033°E, 24.750°N	200	L (0-18)	Xiao et al., 2007
12	TS (Toushe)	120.883°E, 23.817°N	650	L, P (1-73)	Liew et al., 2006
13	GY (Gaoyao)	112.333°E, 22.901°N	16	P (0-6)	Peng et al., 2015
14	DY (Dongyuan)	120.833°E, 22.167°N	330	L (0-22)	Lee and Liew, 2010
15	HML (Huguangyan)	110.283°E, 21.153°N	87	L (0-20)	Sheng et al., 2017
16	SC (Shuangchi)	110.183°E, 19.951°E	90	L (0-8)	Zheng et al., 2003
17	NPK2 (Nong Pa Kho)	102.933°E, 17.102°N	180	L (0-36)	Penny et al., 2001

*Type of archive: P=peat; L=lacustrine

The chronology for the GT core was based on 10 AMS ^{14}C dates (Fig. 2, Table 2). For the SZY core, new ^{14}C dates were obtained and additional pollen analyses carried out to improve the temporal resolution, especially for the late glacial and deglacial intervals. To incorporate age uncertainties associated with the resolution of pollen sampling, Bayesian estimation was applied to age model outputs using the Bchron package in R statistical software (Parmell et al., 2008). This provided probability distribution over the mean age of transitions between successive sampling levels. All ^{14}C dates were calibrated to calendar years using IntCal13 (Reimer et al., 2013). Median values were used for interpolation at different sample depths, except for the transition from the last glacial to the Holocene in the SZY core, where 90% quantiles were assumed between the two dating points.

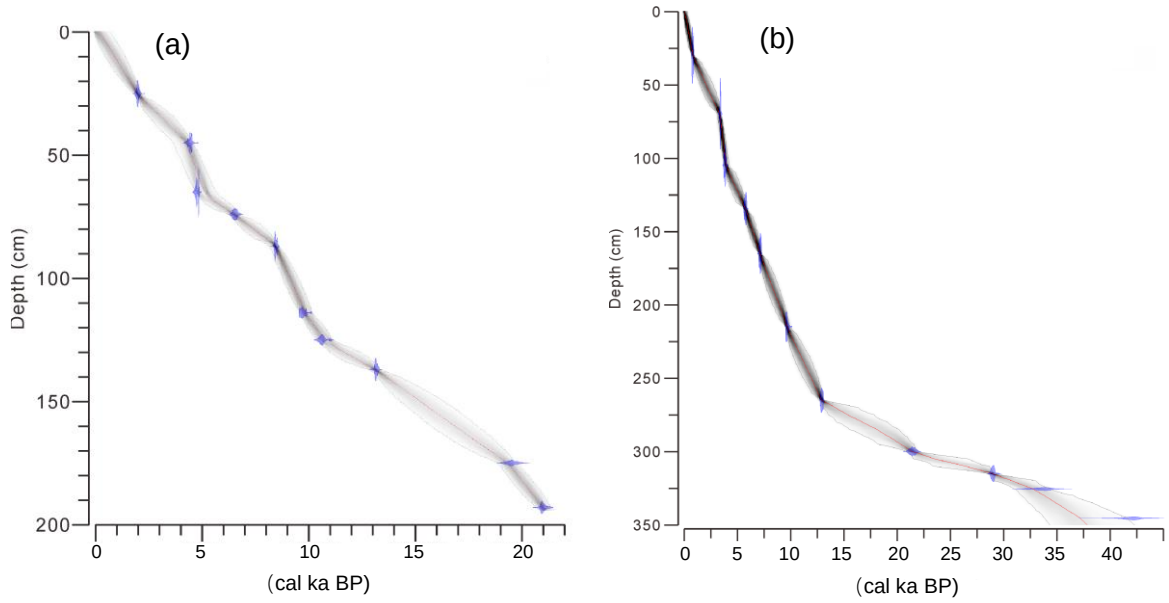

Fig. 2. Age-depth model of the GT (**a**) and SZY (**b**) cores.

Table 2. AMS ^{14}C dates and calibrated ages for the GT and SZY cores

Core	Depth (cm)	Laboratory* Number	Dated material	Radiocarbon age (a BP)	Calibrated age (cal. a BP)
GT	25	Beta-440773	Bulk sediment	2030 ± 30	1907-2090
	45	Poz-84956	Pollen	3970 ± 40	4299-4522
	64	XA 6643	Bulk sediment	4233 ± 28	4662-4850
	74	Poz-84957	Pollen	5740 ± 70	6384-6695
	87	Beta-326017	Bulk sediment	7600 ± 40	8390-8534
	114	XA 6639	Bulk sediment	8738 ± 43	9568-9891
	125	Poz-84958	Pollen	9390 ± 70	10422-10984
	137	Beta-326015	Bulk sediment	11210 ± 60	13025-13237
	175.5	Poz-84960	Pollen	16170 ± 140	19148-19861
	192	XA 6638	Bulk sediment	17395 ± 66	20813-21181
SZY	30	Beta-440771	Pollen	890 ± 30	738-903
	70	Beta-324767	Bulk organic matter	3170 ± 30	3347-3447
	105	GZ 4920	Bulk organic matter	3555 ± 35	3729-3953
	134.5	Poz-84961	Pollen	5020 ± 40	5661-5888
	165	GZ 4922	Bulk organic matter	6230 ± 35	7023-7245
	215	GZ 4921	Bulk organic matter	8690 ± 45	9553-9814
	245	Beta-324765	Bulk organic matter	9240 ± 40	10240-10440
	265	GZ 4860	Bulk sediment	11000 ± 60	12747-13016
	277.5	Beta-469574	pollen	24700 ± 100	28470-28980
	284.5	Beta-469575	pollen	22400 ± 90	26371-27076
	290	Beta-324768	Wood fragment	8430 ± 40	9410-9529
	300	Poz-84966	Pollen	17700 ± 120	21075-21742
	315	GZ 4923	Bulk sediment	24770 ± 110	28620-29004
	325.5	Poz-84968	Pollen	29320 ± 610	31791-34435
	333	Beta-324766	Wood fragment	21880 ± 100	25883-26352
	345.5	Poz-84969	Pollen	37900 ± 1100	40117-43875

358	GZ-4859	Bulk sediment	41680 ± 3380	40480-50301

*Beta, Beta Analytic Inc.; Poz, Poznan Radiocarbon Laboratory; XA, Xi'an Institute of Earth and Environment, Chinese Academy of Sciences; GZ, Guangzhou Institute of Geochemistry, Chinese Academy of Sciences

Following a preliminary examination of a broader fossil pollen dataset (Cao et al., 2013; Penny et al., 2001; Zheng et al., 2016), we selected records from sites in relatively closed basins (upland lakes or marshes) within the subtropical zone with a reliable age model for comprehensive regional analysis. Pollen records from of alluvial, deltaic and river-fed lacustrine sedimentary materials were excluded due to the uncertainty of pollen sources transported by rivers. Thus, only 14 well-dated pollen records (Table 1) were used for regional data integration. Of the selected records, pollen analysis from GT, SZY, JXA, NT and DJH cores were conducted by our laboratory (Yue et al., 2012; Li et al., 2013; Han et al., 2016).

2.2. Methods

We analyzed pollen in samples from several cores collected from the subtropical zone after preparation following standard techniques (Faegri and Iversen, 1989) with minor amendments. Each sample consisted of 2–3 g of sediment and after chemical treatment approximately 500 pollen grains were counted and classified in most samples. The pollen total used for percentage calculations was based on the total number of pollen grains counted, excluding aquatic pollen and spores, and percentages of pteridophyte and fungal spores were based on total counts of palynomorphs. Pollen taxa were grouped by ecological affinity and distribution of parent plants. Pollen groups classified by plant ecological affinity were used to summarize structural-functional changes in the vegetation, with no pollen taxon assigned to more than one group. We summed relative values for the following groups: cold-tolerant conifers, temperate deciduous broadleaved trees, subtropical evergreen

broadleaved trees, eurythermic and subtropical warm conifers, forbs, and wetland plants. For comparative study of regional variation trend, the percentages of arboreal pollen group of evergreen broadleaved trees (EBT) in the selected lacustrine pollen records were standardized by rescaling to values from 0 to 1, and the tropical records (from three sites) and subtropical records (from 14 sites) were separately combined. The EBT pollen data from temperate zone were not used for synthetic analysis because the dominant component is always deciduous taxa rather than evergreen.

To illustrate spatiotemporal vegetation changes in the study area, we used biomes that are geographically and climatically distributed in broad physiognomic zones. Pollen-based biome reconstruction has been successfully performed by applying the biomization technique to various plant functional type (PFT) schemes (Yu et al., 2000; Chen et al., 2010). A recently described scheme for converting pollen taxa to biomes, with some modifications to the PFTs to suit the particular subtropical situations in China (Ni et al., 2014) and adjacent islands (Lee and Liew, 2010; Gotanda et al., 2002) was applied to the GT, SZY and other records. Essentially, we applied a biome PFT taxon matrix previously developed for East Asia (Ni et al., 2014), apart from the exclusion of some PFTs from high-latitude Arctic and boreal zones, such as Arctic shrub, boreal summergreen, and conifers PFTs. The biome taxa matrix was then simplified to focus on the subtropical region that includes locations of the fossil pollen sites. In total, 136 pollen taxa were assigned to 18 PFTs (Table 3). The defined composition of each biome in terms of PFTs is given in Table 4, and 9 biomes from the study area was used. In accordance with previous modifications of the subtropical zone biome, ts2 (a PFT characterized by *Alnus* and *Fagus*) as proposed by Yu et al. (2000) was assigned exclusively to the DBLF biome. The alpine shrub-land biome (ALSH) (Lee and Liew, 2010), characterized by

subtropical mountain vegetation, was also included. The results of biome reconstruction for modern pollen spectra indicate that most samples are correctly assigned. The improved result of biome reconstruction has good correspondence with the present-day vegetation distribution across eastern China (Fig. 3), and some exceptions from the northern subzones of subtropical regions show a dominance of DBLF and CLMX biomes caused by temperature gradients in mountainous regions (samples below 800 m were deleted due to strong human disturbance). We used the difference in biome scores between EBLF and DBLF (E-T) to evaluate the biome shifts.

Table 3. Assignment of pollen taxa from southern China to plant functional types (PFTs) for biomization.

Code	PFT	Pollen taxa
bec	Boreal evergreen conifer	*Abies*, *Picea*, *Pinus* (Haploxylon)
ctc	Cool-temperate conifer	*Abies*, *Tsuga*
ec	Eurythermic or heliophilous conifer	Cupressaceae, *Pinus*
ts	Temperate summergreen	*Acer*, Araliaceae, *Betula*, *Buxus*, *Carpinus*, *Cornus*, *Corylus*, *Euphorbia*, *Fraxinus*, *Galium*, *Quercus* (deciduous), Rhamnaceae, *Rhus*, Rosaceae, Rubiaceae, Rutaceae, *Salix*, *Sambucus*, *Spiraea*, *Tilia*, *Viburnum*
ts1	Intermediate-temperate summergreen	*Alnus*, Caprifoliaceae, *Carpinus*, *Carya*, *Celtis*, *Fagus*, Hamamelidaceae, *Hedera*, *Juglans*, *Liquidambar*, Mimosaceae, *Myrica*, *Nyssa*, *Pterocarya*, Thymelaeaceae, *Ulmus-Zelkova*, Urticaceae, *Vitis*
ts2	Warm-temperate summergreen	Ebenaceae, Elaeagnaceae, *Engelhardtia*, *Platycarya*, *Pterocarya*, *Rhus*
wtc	Subtropical evergreen conifer	*Cephalotaxaceae*, *Dacrydium*, *Keteleeria*, *Podocarpus*, Taxodiaceae
wte	Subtropical broadleaved evergreen	*Altingia*, Anacardiaceae, *Antidesma*, *Aporosa*, Araliaceae, Berberidaceae, *Breynia*, *Buxus Camellia*, *Castanopsis-Lithocarpus*, Celastraceae, *Claoxylon*, Cucurbitaceae, *Cyclobalanopsis*, *Elaeocarpus*, *Engelhardtia*, *Eriobotrya*, Euphorbiaceae, *Eurya*, Fabaceae, Gesneriaceae, Hamamelidaceae, Lauraceae, *Mallotus*, Malvaceae, Melastomataceae, Meliaceae, Mimosaceae, Moraceae, Myrtaceae, Oleaceae, Papillonaceae, *Phylanthus*, *Polygala*, Proteaceae, *Pterospermum*, *Reevesia*, Rhamnaceae, Rubiaceae, Rutaceae, Sapindaceae, Solanaceae, *Symplocos*, *Ternstroemia*, *Tetracentron*, Theaceae
sse	Southern subtropical evergreen	Apocynaceae, *Castanopsis/Lithocarpus*, Celastraceae, Cucurbitaceae, Euphorbiaceae, *Exoecaria*, Fabaceae, *Flacourtia*, Hamameliaceae, Loranthaceae, Lythraceae, *Mallotus*, Malvaceae, Meliaceae, *Nyssa*, Papilionaceae, Sapindaceae, *Symplocos*, *Tilia*, Vitaceae
te	Tropical evergreen	Anacardiaceae, *Antidesma*, Apocynaceae, *Aporosa*, Araceae, Araliaceae, Berberidaceae, *Camelia*, *Claoxylon*, *Eurya*, *Ficus*, Lauraceae,

		Macaranga, Melastomataceae, Mimosaceae, Moraceae, Myrtaceae, Olacaceae, Oleaceae, *Phylanthus*, Proteaceae, *Pterospermum*, Solanaceae, Verbenaceae
tr	Tropical raingreen	Apocynaceae, *Aphanamixis*, *Celtis*, *Dalbergia*, Euphorbiaceae, *Exoecaria*, Fabaceae, Flacourtiaceae, Lythraceae, *Mallotus*, Malvaceae, Meliaceae, Myrsinaceae, *Nyssa*, Papilionaceae, Sapotaceae, *Tilia*
suf	Subtropical forb/shrub	Apiaceae, Araceae, Asteraceae (spiny), Campanulaceae, Solanaceae, Convolvulaceae, *Ilex*, Fabaceae, *Symplocos*, Verbenaceae
sf	Steppe forb/shrub	Amaranthaceae-Chenopodiaceae, Apiaceae, *Artemisia*, Asteraceae, *Astragalus*, Brassicaceae, Campanulaceae, Cannabaceae, Caryophyllaceae, Convolvulaceae, Elaeagnaceae, *Euphorbia*, Fabaceae, *Gentiana*, Labiatae, Liliaceae, Onagraceae, *Plantago*, *Polygonum*, Primulaceae, Ranunculaceae, Rosaceae, *Rumex*, Rutaceae, *Thalictrum*, *Verbascum*, *Xanthium*, *Zanthoxylum*
af	Alpine forb/shrub	Apiaceae, *Artemisia*, Asteraceae, Boraginaceae, Brassicaceae, Caryophyllaceae, Crassulaceae, Fabaceae, *Gentiana*, Geraniaceae, Gesneriaceae, *Impatiens*, Labiatae, Onagraceae, Papaveraceae, Papilionaceae, *Pedicularis*, *Plantago*, *Polygala*, *Polygonum*, *Potentilla*, Primulaceae, Ranunculaceae, Rosaceae, *Sanguisorba*, *Thalictrum*, *Verbascum*, *Viburnum*
h	Heath	Ericaceae, *Rhododendron*
g	Grass	Poaceae
s	Sedge	Cyperaceae

203 **Table 4.** Assignments of plant functional types to biomes.

Code	Biome	Plant functional type (PFT)*
ALSM	Alpine shrub-land, meadow/tundra	af, g, h, s
CLMX	Cold mixed forest	ctc, ec, ts1
COMX	Cool mixed forest	bec, ctc, ec, h, ts
DBLF	Temperate deciduous broadleaved forest	ctc, ec, h, ts, ts1, ts2
EBLF	Subtropical evergreen broadleaved forest	ec,te, tr, ts2, wtc, wte
STEP	steppe	g, sf
TDFO	Tropical dry forest/savanna	g, tr
TRFO	Tropical rainforest	te, sse, suf
TSFO	Tropical seasonal forest	tr, suf, wtc

* PFT codes: bec, boreal evergreen conifer; ctc, cool-temperate conifer; ec, eurythermic or heliophilous conifer; ts, temperate summergreen; ts1, intermediate-temperate summergreen; ts2, warm-temperate summergreen; wtc, subtropical evergreen conifer; wte, subtropical broadleaved evergreen; sse, southern subtropical evergreen; te, tropical evergreen; tr, tropical raingreen; suf, subtropical shrub/forb; sf, steppe forb/shrub; af, alpine forb/shrub; h, heath; g, grass; and s, sedge.

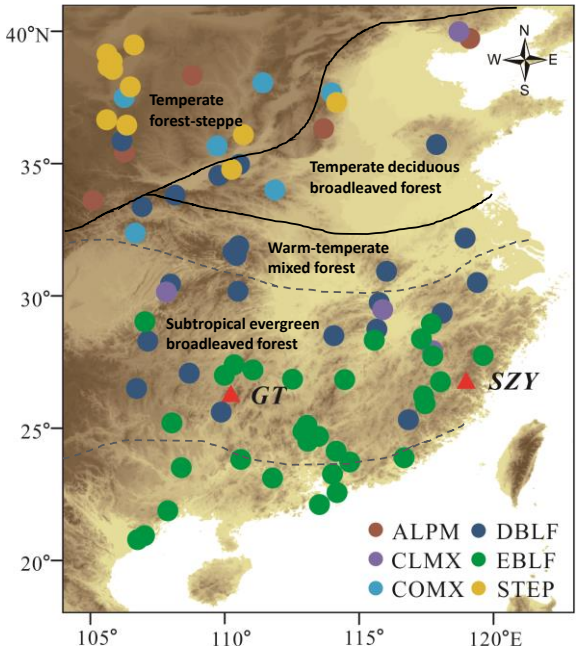

204

205 **Fig. 3. Predicted biomes for modern pollen surface samples from latitudes of 20°N to 40°N in eastern China.** Some

206 samples from the north and northwestern subzones of subtropical regions show a dominance of DBLF and CLMX

207 biomes caused by vertical temperature lapse rate in mountainous localities.

208 We applied the transfer function method to reconstruct the paleoclimate quantitatively from the

209 SZY pollen record, using the Locally-Weighted Weighted-Averaging (LWWA) model (Juggins and

210 Telford, 2012; Juggins and Birks, 2012). Modern pollen data were extracted from the recently

211 updated Eastern Asia Pollen Dataset (EAPD) (Zheng et al., 2014; Zheng and Huang, 2022), with the

212 addition of some recently completed samples. An area in mainland China between 20°-40° N latitude

213 and 105°-120° E longitude around the research site (SZY) was selected (Fig. 4). We screened the

214 modern samples and excluded those that had clearly been disturbed by human activities, leaving 683

215 surface samples for use in the calculations. The climate at each modern site was interpolated from

216 modern climatic data of 756 meteorological stations in the years of 1981-2010 in China

217 (http://data.cma.cn). The thin plate spline regression was applied in the interpolation process for each

218 modern pollen site. The robustness of the transfer function model was assessed by calculating the

root mean square error of prediction (RMSEP) and coefficient of determination (R2) between measured and predicted values. The R software package (Juggins, 2017) was used to calculate the pollen-climate model.

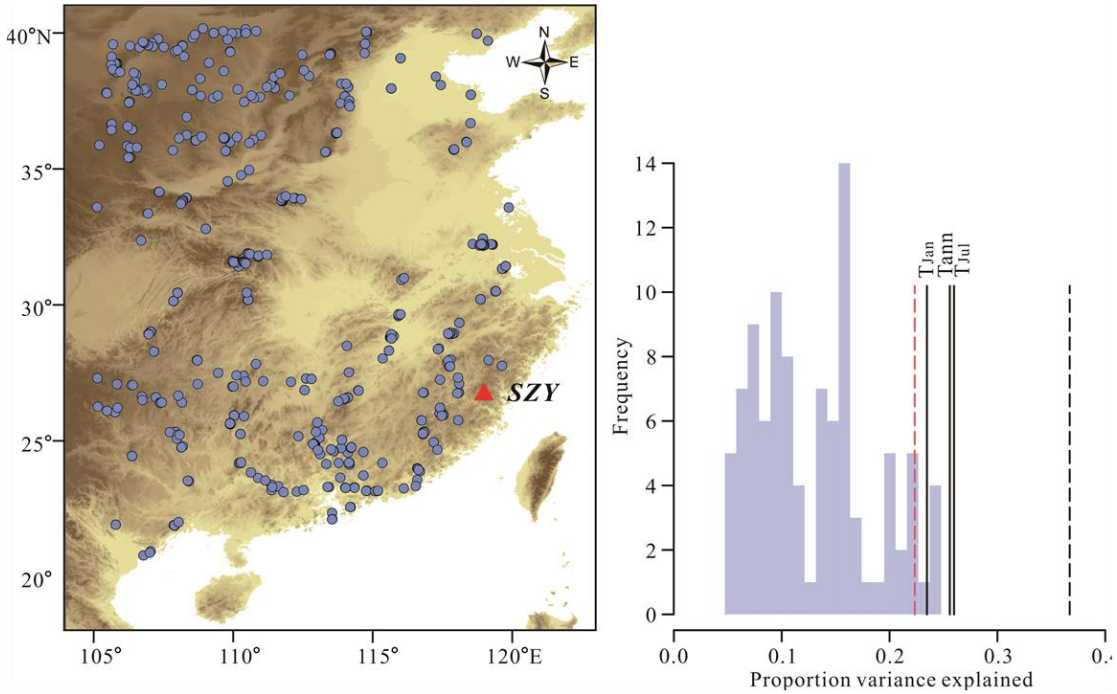

Fig. 4. Modern pollen samples (left; gray circles) and a significance test for the pollen-based climate reconstructions (right). The red triangle indicates the location of the SZY core. Gray bars indicate the proportion of variance, and the red dotted line indicates the proportion of variance below which 95% of the random data-trained calibration functions can be explained.

We use the branched glycerol dialkyl glycerol tetraether (brGDGT) as an independent method to quantify past temperature changes (Wang, et al., 2017). Samples for biomarker analysis were taken from the same core (SZY) of pollen analysis, which was measured using high-performance liquid chromatography/atmospheric pressure chemical ionization-mass spectrometry. GDGTs were detected by using the selected ion monitoring (SIM) mode, following the methods described by Schouten et al. (2007). The quantification of GDGTs was achieved by integration of the peak area of

233 $[M+H]^+$ ion traces of branched GDGTs. Replicate HPLC/APCI-MS analysis of more than 10
234 samples showed the reproducibility of MBT'(Methylation index of Branched Tetraethers), which
235 was used for calculating the annual mean temperature with the equations given by Weijers et al.
236 (2007) and Peterse et al. (2012).

237 For climate simulation, we use the TRACE21 model at the T31 spatial resolution (3.75°x3.75°),
238 which is the first state-of-the-art transient simulation of global climate change over the last 21 ka
239 (Liu et al., 2009; 2012). We selected an area covering 22°-27° N to 105°-120° E to represent
240 subtropical southern China to compare results of the simulations with corresponding proxies. The
241 simulated local climate variables of the studied sites were extracted directly from the corresponding
242 spatial grids simulated by TRACE21 model (Liu et al., 2009). Six climatic variables are analyzed:
243 annual mean precipitation and mean temperature, mean winter (December-February) and summer
244 (June-August) temperatures, and indices of temperature and precipitation seasonality (corresponding
245 to WorldClim bioclimatic variables 4 and 15) (Hijmans et al., 2005). These variables were chosen
246 because they provided the maximal explanatory power of potential predictors, although some co-
247 linearity was still present, especially for winter temperature and temperature seasonality.

248

249 **3. Results and discussion**

250 *3.1. Pollen records and biome reconstructions*

251 We regard results from the two high-resolution pollen records as representative of vegetation
252 changes in the middle subtropical zone during the last glacial-interglacial transition. Both records

indicate a substantial change in distribution of the subtropical ecosystem from the LGM at 22 ka BP to the Holocene. The pollen at the LGM at sites of the two records was dominated by cold-tolerant, temperate broadleaved forest taxa (*Fagus*, *Carpinus*, *Betula*, *Corylus*, *Juglans* and deciduous *Quercus*), mixed with cold-tolerant alpine conifer taxa (*Tsuga* and *Abies*), indicating that temperatures were much lower than today (Figs. 5 and 6). During the Bölling/Alleröd (B/A) warm period (15.5-13 ka BP), there was an early increase in pollen of the evergreen forest tree genus *Cyclobalanopsis*. However, the taxa *Castanopsis/Lithocarpus* and *Altingia* increased significantly and reached dominant percentages until the middle Holocene at both sites. Among the non-arboreal pollen (NAP) taxa, Poaceae was the most abundant, and tended to increase, reaching maximum percentages in the late Holocene. Cyperaceae, a wetland plant, began to increase at ca.12 ka and peaked in the mid-Holocene, positively correlating with pollen taxa of evergreen broadleaved trees.

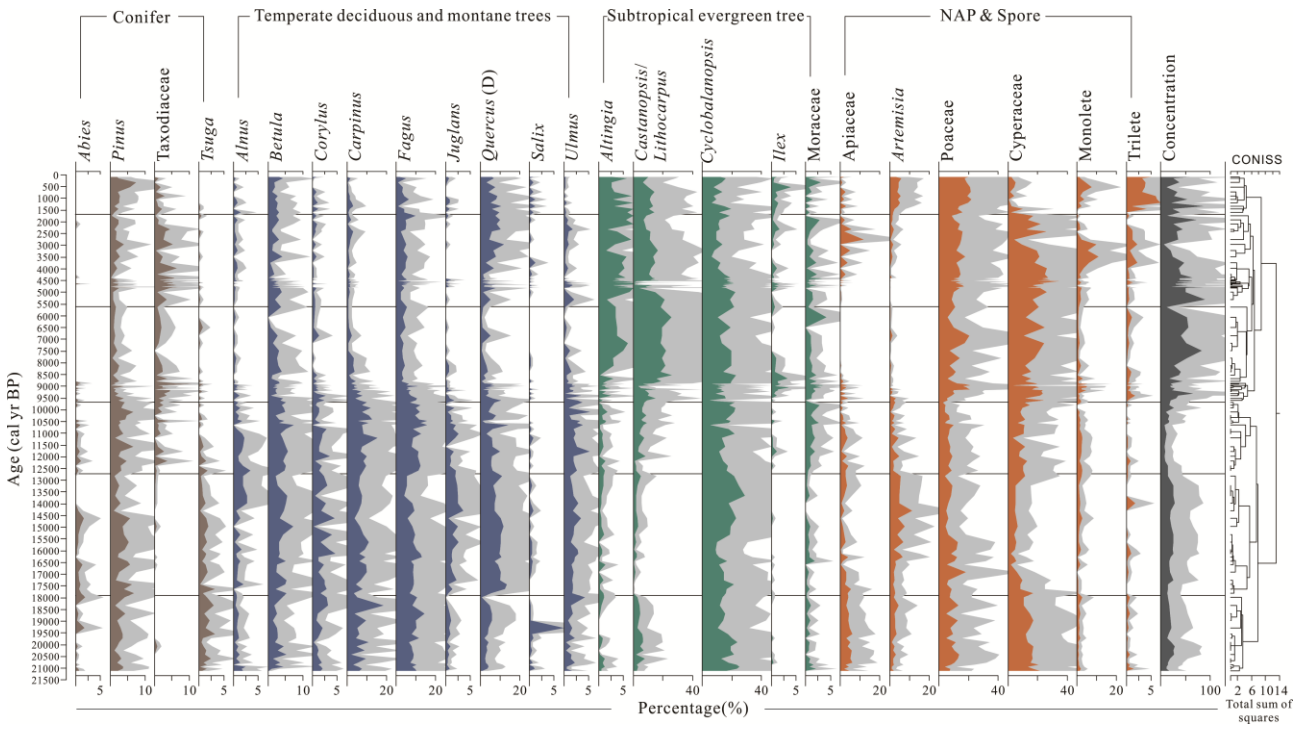

Fig. 5. Detailed pollen diagram of selected taxa from the GT core. Percentages were calculated from the sum of all pollen grains counted. The unity of pollen concentration is the count number per gram ($\times 10^4$).

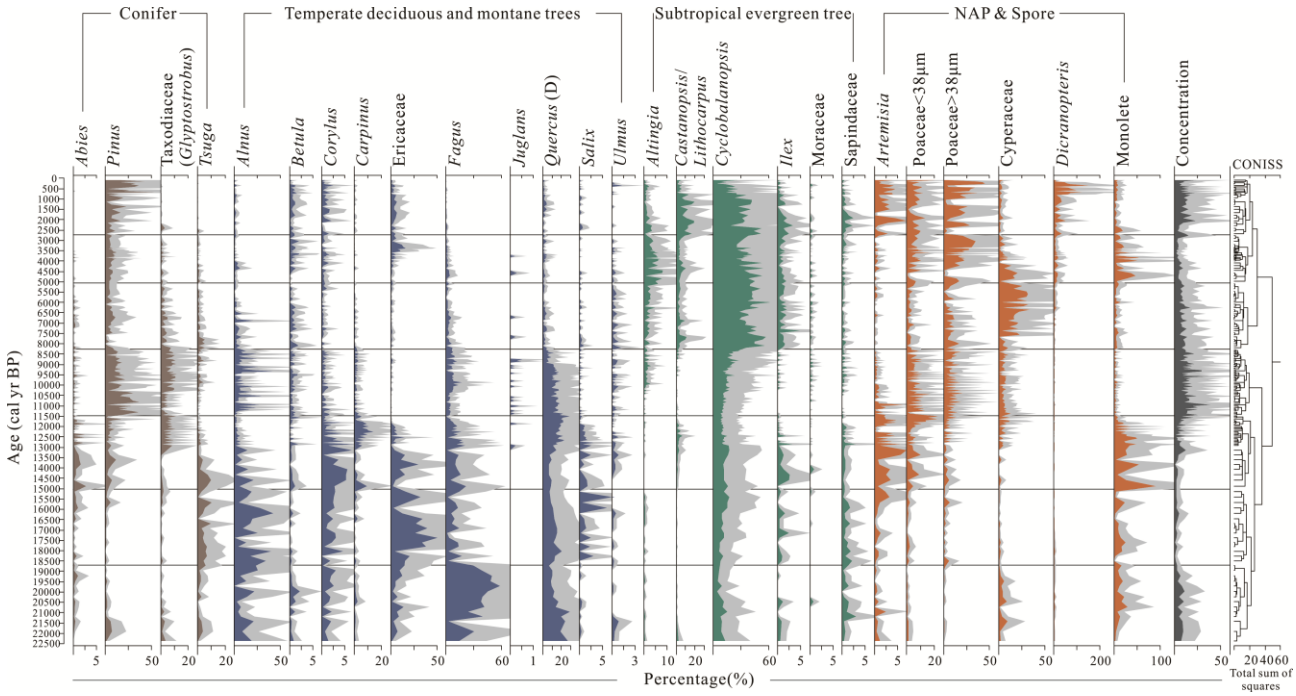

Fig. 6. Detailed pollen diagram of selected taxa from the SZY core. Percentages were calculated from the sum of all pollen grains counted. The unity of pollen concentration is the count number per gram ($\times 10^4$).

We used pollen groups classified by plant ecological affinity to synthesize the taxonomic pollen data (Fig. 7), and reconstructed biomes using the biomization technique (Yu, et al., 2000) based on its successful application with modern pollen samples (Fig. 3). Arboreal taxa of the two pollen records indicated the dominance of temperate deciduous broadleaved trees (DBT), corresponding to the DBLF biome, during the glacial and early Holocene periods. Such temperate deciduous forest vegetation indicates glacial climatic conditions different from those of today in the subtropical zone. During the Bölling/Alleröd (B/A) warm period (16-13 ka), there was a moderate increase in pollen group of evergreen broadleaved trees (EBT). The primary increase in evergreen broadleaved tree (EBT) during the B/A was more pronounced at SZY than GT, reflecting the difference in sites' elevation (1007 and 1677 m asl, respectively). The biomization result shows that the evergreen forest biome (EBLF) during the last glacial and early deglacial periods did not exceed those of temperate deciduous broadleaved

forest (DBLF). The primary increase in broadleaf evergreen forest components since the last deglaciation was interrupted during the cold Younger Dryas (YD). Such an abrupt change was also marked by increases in forbs and sedges, reflecting drier condition on land and locally shallowing lake waters. After the YD, EBT forest group slowly increased again from about 11.3 ka, and biome change from DBLF to EBLF occurred at 8.7 ka in GT and 8.1 ka at SZY (Fig. 7), reflecting a time difference between latitudinal locations. In particular, the reconstructed biome changes during the mid-Holocene showed that the decrease in DBLF was more significant than the increase in EBLF. There was also only a marginal dominance of EBLF or a mixed EBLF and DBLF biome at sites characterized by relatively high elevation and low air temperature, such as GT (1677 m asl), during the middle to late Holocene. This elevational effect suggests that deglacial migration of vegetation occurred not only along a north-south latitudinal transect but also along an elevational gradient. Over the last 4,000 years, EBLF decreased relative to DBLF, indicating that the forest type was more consistent with the evergreen/deciduous mixed forest since then. In addition, the abundance of non-arboreal taxa (forbs) increased progressively in both records, suggesting a drying trend that probably had interactive effects with anthropogenic influences, at least within the last 2 ka (Ma et al., 2018).

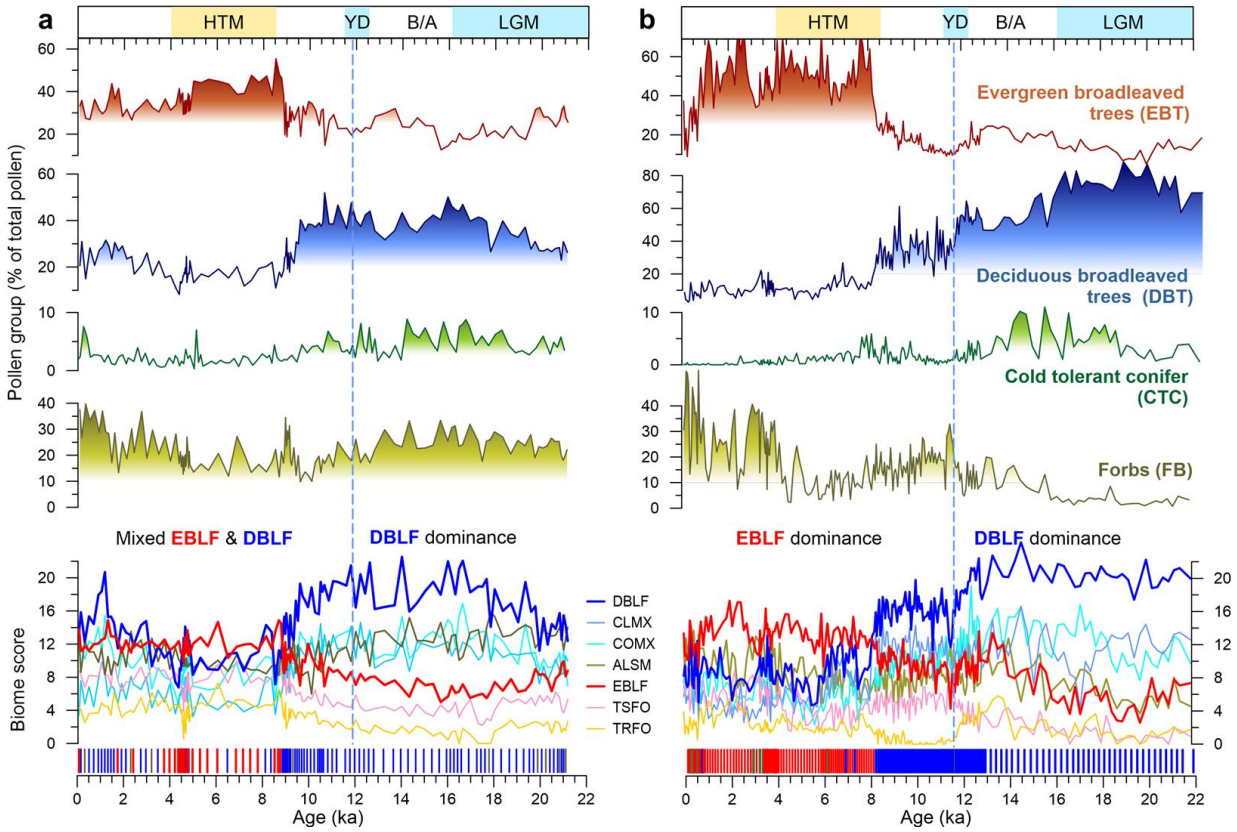

Fig. 7. Pollen groups and reconstructed biomes for the last 22 ka based on the GT (a) and SZY (b) cores from the middle subtropical zone. Percentages (of total pollen grains) counted of the following four pollen groups are shown: evergreen broadleaved trees, deciduous broadleaved trees, cold-tolerant conifers and terrestrial forbs. The biomes shown in the lower panels are temperate deciduous broadleaved forest (DBLF), cold mixed forest (CLMX), cool mixed forest (COMX), alpine shrub and meadow/tundra (ALSM), subtropical evergreen broadleaved forest (EBLF), tropical seasonal forest (TSFO) and tropical rainforest (TRFO) (Table 3).

3.2. Quantitative climate reconstruction and comparison with simulation result

We applied a quantitative method to reconstruct the paleoclimate from the SZY pollen record. The mean annual temperature (Tann), which may strongly influence regional forest distributions, passed the significance test for the reconstruction (Fig. 4). We selected annual mean temperature as the representative parameter to explore the vegetation-climate relationship. The result shows that the

estimated Tann from the SZY fossil pollen record was lowest (about 8°C) during the LGM, and it increased to 15–17°C during the mid-Holocene, with an amplitude in variation of up to ~8°C between the glacial and postglacial periods (Fig. 8). The reconstructed temperatures below 12°C during the glacial period from 22 ka to 15 ka are consistent with conditions suitable for the deciduous forest biome, but far from the threshold temperatures required by evergreen forest. This quantitative estimate falls within the framework of previously simulated temperature using climate models, showing that in subtropical areas annual climatic conditions for deciduous forest expansion during the LGM could include annual temperatures as low as 11°C (Ju et al., 2007; Tian and Jiang, 2016). According to the reconstruction there was a temperature rise at 15 ka, corresponding with the B/A warming. However, after the YD the rate of warming in the SZY locality slowed, with fluctuations, and only increased rapidly to near the EBLF threshold temperature (>15°C) after the 8.2 ka event. The perfect match of quantitative climate data with biome changes revealed that the temperature threshold leading to EBLF as the dominant forest was about 15–17°C in the mountains of the middle subtropical zone. It should be noted that both the SZY and GT sites are on summits of subtropical mountains, which may receive pollen carried by upward wind from nearby lower forest belts.

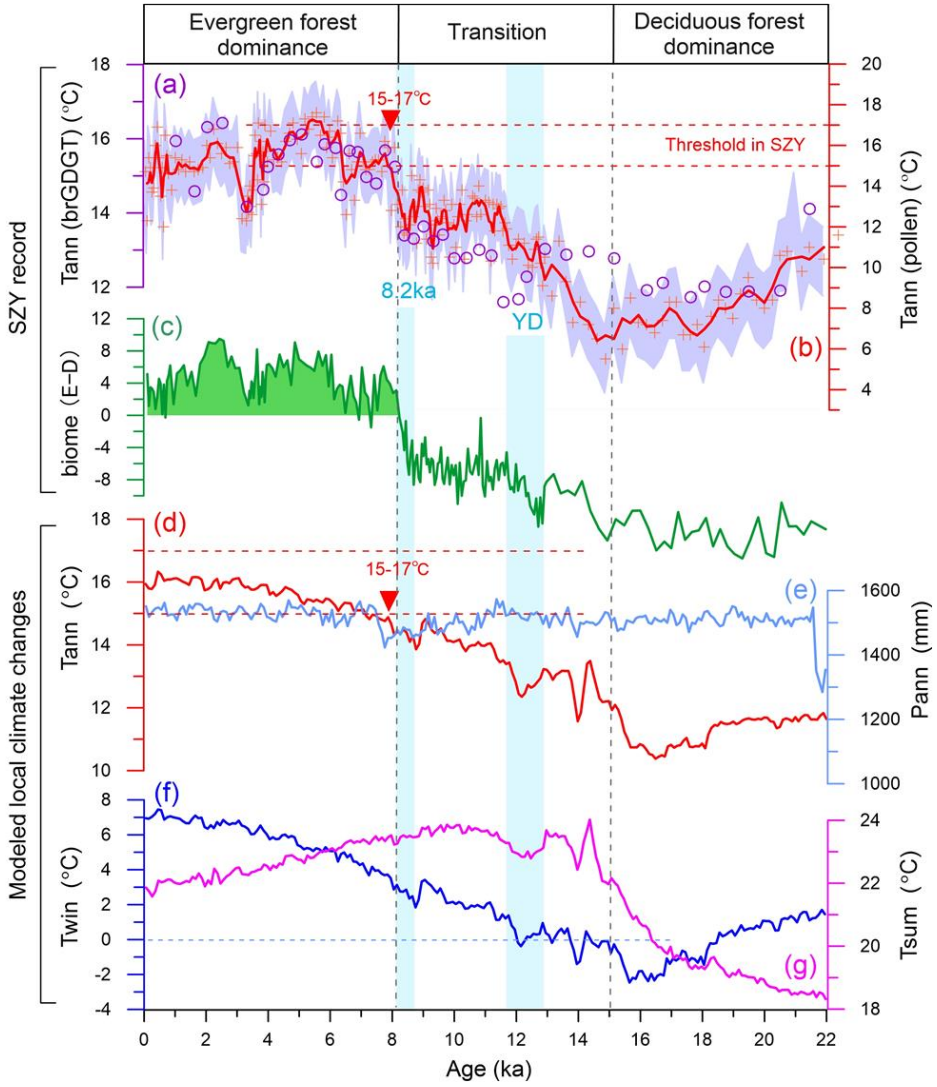

Fig. 8. Reconstructed and modeled temperatures compared with biome changes in the SZY record. (**a)** brGDGT-based mean annual temperature reconstruction (Wang et al., 2017) (purple circles) coupled with (**b)** pollen-based annual temperature reconstruction (red line of smoothed data over the grey error range), showing local temperature threshold range for EBLF (red dotted line). (**c)** Biome changes as indicated by the difference between evergreen and deciduous biome scores (EBLF-DBLF)**.** Climate simulation by transient model extracted from the grid point at SZY locality: (**d**) annual mean temperature (Tann) and (**e**) annual precipitation (mm). (**f**)Winter (Twin) and (**g**) summer (Tsum) temperatures.

To validate the pollen-based temperature proxy, we performed a parallel reconstruction of air

temperature from the same core (SZY) using brGDGT (Wang et al., 2017), as an independent climate reconstruction method. The brGDGT-based Tann indicated a rapid increase 13°C to >15°C at ~8.1 ka, which is largely consistent with the pollen-based climate reconstruction. Similar degrees of variation and thresholds apply to the two temperature proxies, particularly for the key timing of the YD event and the substantial forest transformation starting at ~8.1 ka, despite some differences between absolute values of the LGM derived by the two methods. Overall, there is strong agreement between forest transitions and quantitative climate changes derived from pollen and other biomarkers in the same sediment material (SZY), both long-term (orbital scale) and short-term (rapid shifts, e.g., in the YD event), indicating sensitive response to climate change (Fig. 3). Since about 8.1 ka, tThe reconstructed annual temperature derived from both pollen and branched glycerol dialkyl glycerol tetraethers (brGDGT, see below) remained consistently high in the mid- to late Holocene (15–18°C), since about 8.1 ka, with only a clear cooling event at about 3.5 ka.

We used transient simulation, generated with TRACE21 (Liu et al., 2009), to assess the seasonal and annual climatic changes in the study area during the last 21 ka. The modeled climate data corresponding to the geographical location of the SZY study site were extracted, and systematically corrected according to the present-day local climate observations. The results show that modelled mean annual and winter temperatures, characterized by progressive increase towards the late Holocene, were crucial for changes in forest components (Fig. 8). The simulated mean annual temperature (Tann) threshold for local EBLF as the dominant forest was higher than 15°C, in good agreement with the pollen- and brGDGT-based climate reconstructions. In terms of seasonal climate, a threshold simulated winter temperature of about 4°C for EBLF expansion in subtropical

mountainous areas was obtained. The simulation indicates that precipitation may not be a key factor for the focal forest transformations, because it remained similar during the covered period, with annual rainfall consistently exceeding 1000 mm since the LGM (Fig. 8e). In summary, the model-proxy comparison revealed good consistency for the climate thresholds for local forest transformation from DBLF to EBLF, except for a few differences in the late Holocene.

3.3. Evergreen/deciduous forest alternation since the last glacial maximum across eastern China

Three distinct evolutionary stages of vegetation change over the subtropical zone could be identified (Fig. 8). During the LGM (stage I), the dominant biome was DBLF, with negative score values of biome difference between EBLF and DBLF (E-D) ranging from -15 to -5. During stage II (from 15 to 8.1 ka), this score gradually increased from -10 to +10, most strongly between 11.3 and 8.1 ka. This indicates a transition period characterized by an increase in the evergreen biome to an extent equal to or greater than that of the deciduous biome. However, the score only rose from - 10 to 0 in the SZY and GT records, due to their locations in mountainous areas at altitudes higher than 1000 m. During stage III (after 8.1 ka), substantial evergreen forest recolonization occurred, with E-D scores rising up to +5 to +20. Integration of pollen records from the subtropical region consistently shows that the two abrupt global cooling events (i.e., the YD and 8.2 ka event) had major impacts on the regional vegetation and Asian climate system (Wang et al., 2001; Cheng et al., 2020). Our data from across the subtropical region indicate a period of maximum EBLF dominance between 8 and 5 ka, corresponding to the Holocene Thermal Maximum (HTM). The late Holocene records from the study sites show a decline of EBLF or an unstable fluctuation with complex changes in the local ecosystems, such as a

decline in wetlands, colonization by terrestrial forbs instead of forest trees, and expansion of secondary forest with abundant pioneer ferns (Figs. 5 and 6).

Previously compiled vegetation proxy data suggest that the modern forest distribution in southeastern China does not differ greatly from that of the LGM, and that forest cover has changed little (mostly between 5%) during the last 22 ka (Tian et al., 2016). However, our pollen data and biome reconstruction, which distinguish between deciduous and evergreen forests, suggest a fundamental change in forest type occurred during the last glacial cycle. In this study, we compiled data on pollen groups composed of representative evergreen broadleaved trees from multiple records across the subtropical zone (Fig. 9). The results indicate that an initial increase in EBT during the B/A warming coincided with a peak period in the tropical zone, and hence an early northward expansion of evergreen forests. However, since the YD event, the decline of EBT in the tropics indicates an opposite trend to that of the subtropical zone. Such contrasting trends in EBT between the tropical and subtropical zones since the end of YD can be interpreted as a northward biome migration. The timing of EBLF biome transformation at four locations from 22° N to 27° N latitude shows a successive northward shift, with dates at 11.2, 10.2, 8.7, and 8.1 ka (Fig. 9c), strongly suggesting a time-transgressive pattern. That is, vegetation response to Holocene warming apparently occurred earlier in the southern subzone than in the middle and northern subzones. The results also indicate that the latitudinal limit of the evergreen forest was south of site DJH, located at the northern subtropical boundary (31.5° N latitude and 1751 m asl). Site DJH was not dominated by EBLF during the mid-Holocene, and it is still not dominated by EBLF today, which is not surprising as the current annual temperature (Tann) is about 7–8°C at an elevation of 1700 m, far below the climatic range for EBLF

dominance. The findings suggest that the EBLF's northward migration during the HTM only reached the mountainous regions south of 31° N.

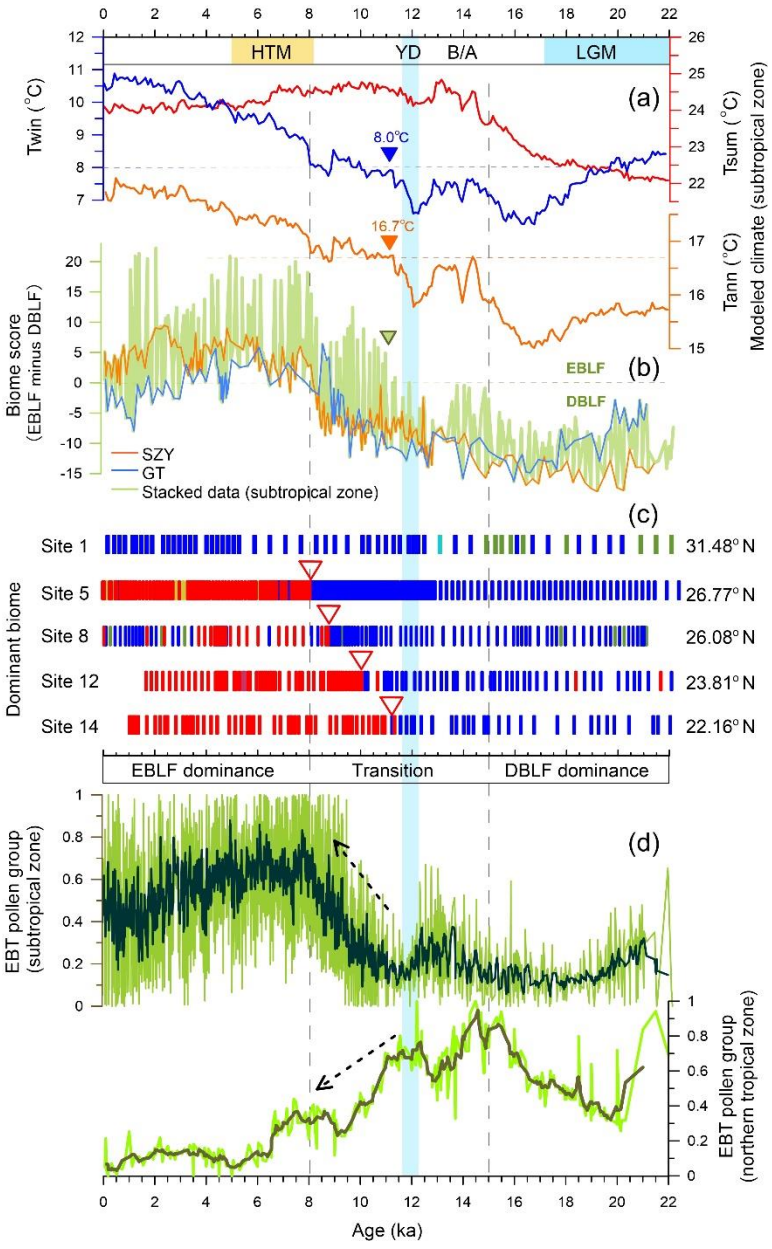

Fig. 9. Relationship between biome and climate changes in the subtropical zone. (**a**) Winter (blue), summer (red) and annual mean (orange) temperatures for the subtropical zone simulated by TRACE21. (**b**) Staked data of regional biome changes showing differences between evergreen and deciduous biome scores (light green), where SZY and GT mountain records are indicated in particular. (**c**) Dominant biome comparison among sites 1 (DJH), 4 (SZY), 7 (GT), 11 (TS) and

12 (DY) (see the legend for biomes in Fig. 7). (**d**) Combined pollen data of the evergreen broadleaved tree (EBT) in the subtropical and tropical zones of the Northern Hemisphere (5-point moving average in brown) (pollen data from each record are standardized to 0-1 values).

In order to reconstruct the regional shifts of EBLF across eastern China and better understand its spatiotemporal changes, we selected a key pollen taxon *Castanopsis/Lithocarpus* which is dominant in evergreen broad-leaved forest for data integration of different climate zones. The taxon of *Quercus* was not used because of the great uncertainty in the identification of pollen taxa at the genus level between evergreen-type and deciduous-type. A total of 108 records from the pollen database in eastern China (Cao et al., 2013; Zheng et al., 2016) have been examined. The data integration results of different climate zones in eastern China (longitude and latitude ranges from 100 to 125°E and from 18 to 40°N) show the increases in *Castanopsis/Lithocarpus* (equivalent to EBLF) since the last deglaciation represent a significant time-transgressive forest response from south to north. The proportion of evergreen forest elements decreased obviously in the northern subtropical subzone, and almost disappeared northward in the temperate zone (Fig. 10). It is clear that the EBLF distribution was restricted to the south of northern subtropical boundary even during the HTM. Besides, the EBLF expansion along altitudinal gradients in mountain ranges of the middle subtropical zone (e.g. GT record at 1677m asl.) also lagged behind those in the southern subtropical lowland regions and/or coastal plains.

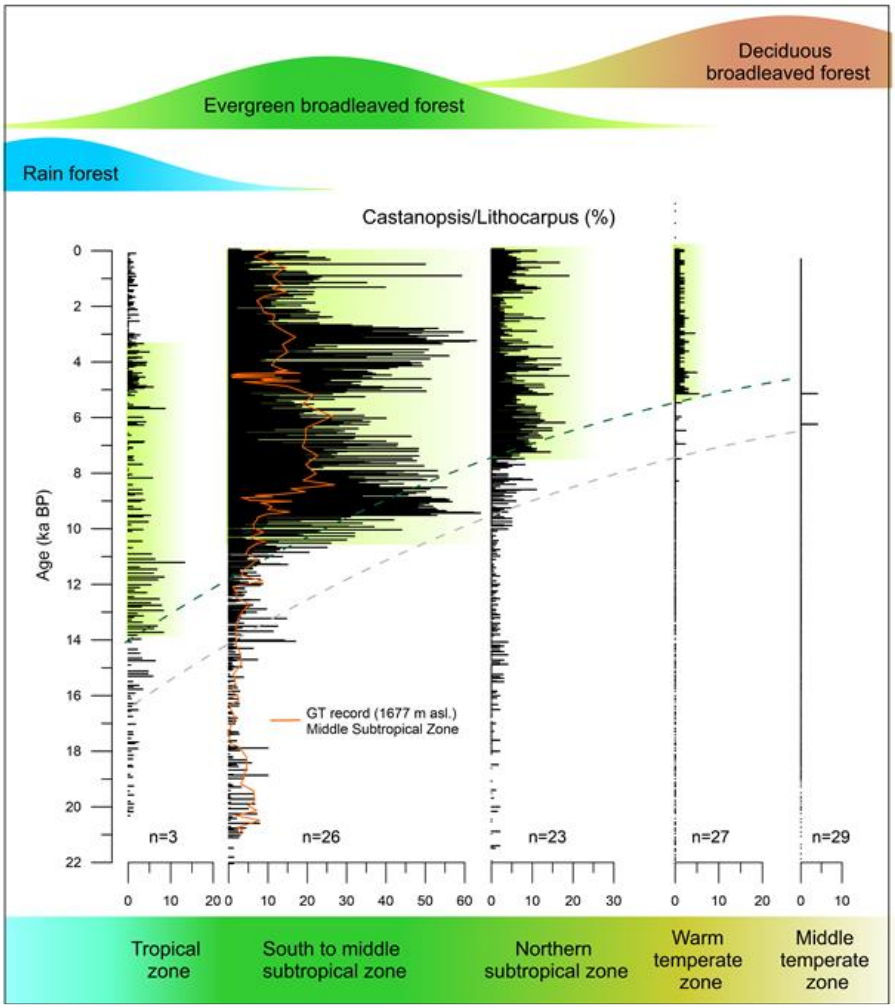

Fig. 10. Synthetic changes of the dominant pollen type of *Castanopsis/Lithocarpus*, a representative taxon in evergreen broadleaved forest, in different climate zones across eastern China over the last 22 ka. The number of records (n) used in each climate zone is shown. The dotted line indicates the early forest response to climate warming and a time-transgressive pattern across eastern China. The orange line is the record from GT mountain peatland at 1677m.

The large-scale biome shifts across eight degrees of latitude, from 22 to 30°N, and the high temporal precision of the fossil record, enabled us to estimate the forest migration rate. Our results indicate that a fundamental biome upheaval began as early as 11.2 ka, initially in the southern subtropical subzone (south of ~22°N). General recolonization of evergreen forests in the middle subtropical mountains

(around 24-28°N) then accelerated during the mid-Holocene (8-6 ka), until the modern northern subtropical boundary was reached at around 6-5 ka. According to the relationship between migration distance and time, the average migration rate was about 155km/ka northward during the transition period from early to middle Holocene.

3.4. Regional climate changes and thresholds leading to EBLF expansion

The general patterns of deglacial warming observed in the climate simulations may help to improve understanding of the forcing and dynamic mechanisms involved in spatial migration history of EBLF. For each individual locality, the EBLF variation in many records shows a rapid change in forest replacement within a relatively narrow time span, suggesting that climatic thresholds may play a key role in forest transformation. Among the bioclimates required for EBLF growth, temperatures are the most important determinants for its boundaries in China (Fang and Yoda, 1991; Hu et al., 2014). Annual and winter temperatures from the transient model over the subtropical zone show consistent variation with integrated subtropical biome changes between deciduous and evergreen broadleaved forests. There was a moderate increase in the modeled temperatures, particularly in summer, during the B/A warming. This resulted in a limited increase in EBLF, mainly in the southeastern and low-altitude parts of the subtropical area near the west Pacific Ocean, such as the Chinese coastal regions and islands (e.g., sites 11 and 12 in Fig. 9c). However, both simulated and proxy climate variables for the mountainous localities in the central subtropical zone (e.g., SZY record) indicate that temperatures remained below the thresholds for evergreen forest transformation during the early deglacial warming

(B/A). Thus, dominance of the deciduous forest biome persisted there. Soon after the YD cooling, simulated temperatures for the subtropical area reached regional mean thresholds of ca.16.7°C (Tann) and 8.0 °C (Twin) (Fig. 9d). Such average climate thresholds for EBLF dominance during the Holocene in subtropical China are highly consistent with current optimum climate conditions for EBLF simulated using the Species Distribution model (Hijmans et al., 2016), with median percentiles of 16.7°C and 8.1°C for Tann and Twin, respectively (Fig. 1c). Our results are also consistent with meteorological data delineating the modern EBLF distribution in the subtropical mountains (Liu et al., 2010). It should be noted that in the vertical and northern boundary areas of the subtropical region, the temperature thresholds for EBLF transformation are slightly lower than the regional averages. For example, records for mountainous parts such as the SZY site (altitude, 1007 m) indicate that the Tann and Twin thresholds are 15 and 4 °C, respectively, and these areas cover roughly 10–30% of the modern EBLF distribution. During the transition period of the early Holocene, the warming reached the thresholds for EBLF dominance earlier in the south than in the north. Such time difference in temperature rises to the threshold along latitude and vertical gradients since the LGM are reflected in delayed biome changes northward. During the early Holocene, temperatures in subtropical Asia gradually increased to levels near the EBLF thresholds. However, temperatures in a large area to the northern boundary of the zone may have still been below the thresholds, resulting in a north-south temperature gradient, and thus there was an earlier forest response at sites along low latitudes as compared to sites located further north. Similar time-transgressive patterns have already been observed in proxy records of the East Asian monsoon region (An et al., 2000; Zhou et al., 2016; Ren and Yi, 2019).

Low winter and/or minimum temperatures compared with summer, linked with the length of the growing season, were likely important constraints on the rate of EBLF migration during this period. A vegetation shift from the early to mid-Holocene triggered by the winter warming effect on vegetation has been corroborated by sensitivity experiments involving rainfall and thermal forcing with a land-vegetation model (Cheng et al., 2021). As well as temperature, mountainous topography in the study area may have also played a role, as a geographic barrier hindering northward biome migration (Xu et al., 2015). Notably, records for site TCK1, at 3898 m asl, indicate that the major forest biome change in the southwestern plateau of China occurred at ~6 ka (Xiao et al., 2014), more than 2,000 years later than at a similar latitude in southeastern China. This may have been a consequence of the temperature lapse rate along the altitudinal gradient, so both latitude and altitude may have geographically influenced temperature gradients and constrained the vegetation belts (Cheng et al., 2018).

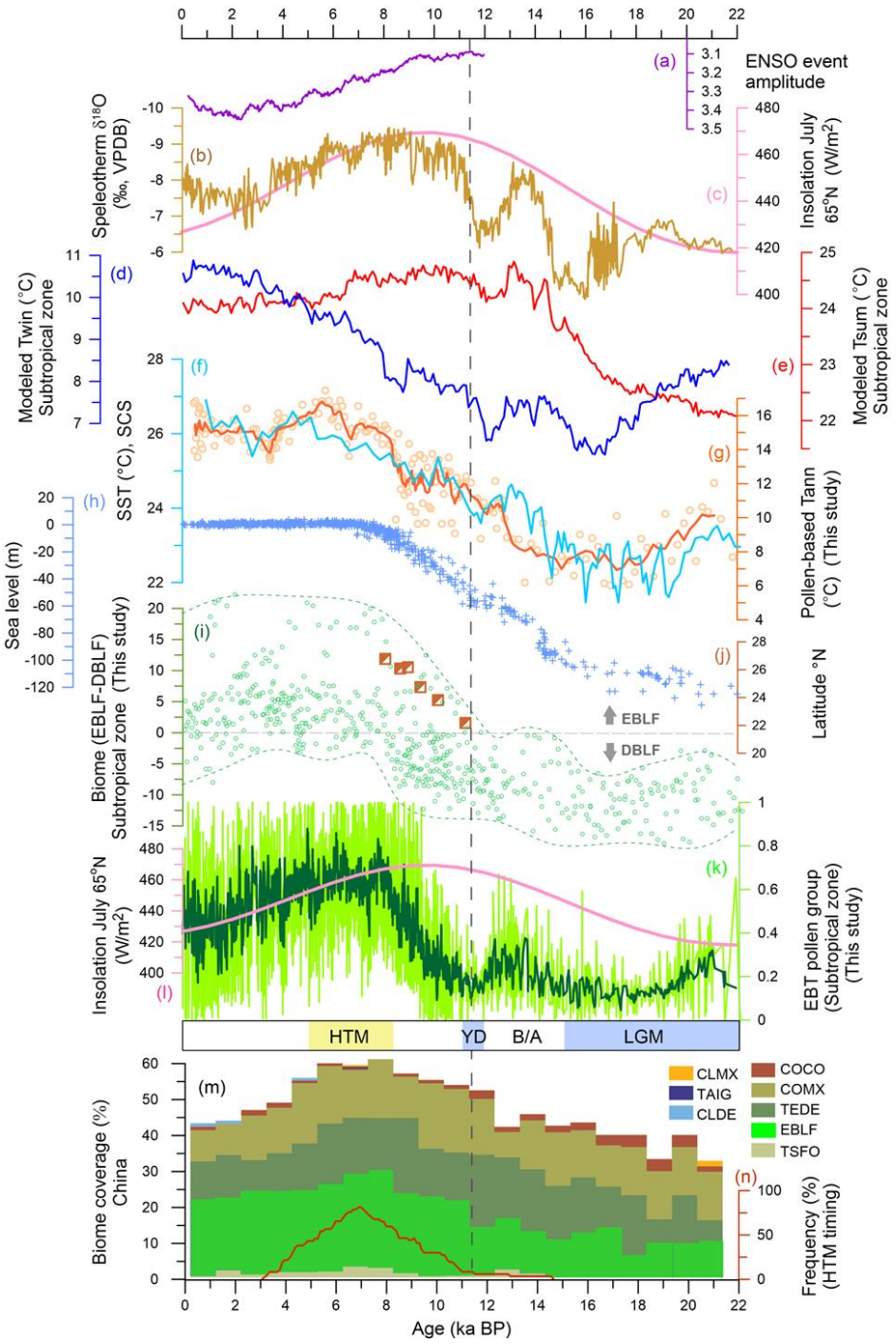

Fig. 11. Comparison of proxy records, simulations and paleoclimate forcings. (a) Mean amplitude of 500-year overlapping windows for ENSO events exceeding 3 k (in °C) (Clement et al., 2000). **(b)** Speleothem oxygen isotopic records from the Hulu and Dongge caves (Wang et al., 2001; Dykoski et al., 2005). **(c)** July insolation at 65°N latitude. **(d)** and **(e)** TRACE21 winter (blue) and summer (red) temperatures for the subtropical zone; **(f)** Alkenone-sea ruface temperature estimates for the northern South China Sea (He et al., 2008). **(g)** Pollen-based temperature reconstruction

(Tann) from the SZY record (the orange line shows the five-point averages). **(h)** Ice-volume equivalent sea level estimate (Lambeck et al., 2014). **(i)** Stacked data of the biome scores (EBLF-DBLF) for the subtropical zone. **(j)** Timing and latitude positions for the EBLF as a dominant forest from record sites 4, 7, 8, 10, 11, 12 (Table 1). **(k)** Standardized values of pollen group of evergreen broadleaved taxa (EBT) in the subtropical zone; **(l)** July insolation at 65°N latitude. **(m)** Proportion of biome coverages in China at 1000-yr resolution (Li et al., 2019). **(n)** Frequency variation of the HTM interval indicated by pollen data in China (Jiang et al., 2019).

Our solid evidence of the subtropical biome shift during the last glacial-interglacial transition enables better understanding of the sensitivity and potential mechanism of vegetation response to global climate change. The observed onset of primary increases in evergreen arboreal elements coincides with the B/A warming during the early deglaciation. The initial gradual increase in EBLF biome coincided with the main phase of deglaciation occurred from ~16.5 ka to ~8.2 ka BP at an average rate of sea-level rise of 12 $m \cdot ka^{-1}$ inferred by Lambeck et al., 2014 since about 16 ka (Fig.11). Effects of changes in land-sea configuration associated with sea-level changes also suggest that internal variability in the climate system linked with global energy fluxes on millennial time scales play important roles in radiative imbalances (Baggenstos et al., 2019), and hence both temperature and vegetation. In addition, coupled trends between temperatures reconstructed from a middle subtropical record and surface temperatures of the northern South China Sea (He et al., 2008) imply a close land-sea relationship and the importance of tropical ocean circulation (DiNezio and Tierney, 2013). Our data reveal that the EBLF distribution peaked in a Holocene interval between 8.1 and 5 ka, associated with the maximum forest coverage in China (Li et al., 2019). Such interval of forest expansion indicates the warmest condition, which is consistent with the HTM, traditionally thought to have occurred during

the mid-Holocene in Asia (Shi et al., 1993; Jiang et al., 2019).

Our analysis shows a time-transgressive pattern of forest replacement from south to north, consistent with the assumption that there was an expansion and/or northward retreat of the Holocene Optimum (Ren and Yi, 2019). Similarly, monsoon precipitation previously reconstructed from pollen data also shows a time-transgressive pattern of maximum precipitation, with earlier occurrence in the southern area and later in the northern area (Zhou et al., 2022). They suggested that the monthly insolation changes force regional climate in different parts of the monsoonal China through a shift in the Western Pacific Subtropical High. In northern China, there was also a delayed ecosystem (tree cover) response to changes of monsoon intensity which was likely caused by winter warming and the subsequent feedback effects on soil moisture (Cheng et al., 2021). In this study, we suggest that temperature change (particularly winter warming) was crucial for the EBLF expansion. Apparently, rainfall in the subtropical mountainous areas of southeast China during the last glacial cycle remained relatively high due to the orographic effects, indicating that precipitation changes may not be a key factor for the EBLF/DBLF alternation. Moreover, simulated variations in precipitation and temperature were not coupled during the early to mid-Holocene.

, implying a gradual weakening of the temperature gradient between high and low latitudes. This may have been related to airflows linked to the Hadley circulation and changes in position of the Intertropical Convergence Zone (ITCZ) (Reimi et al., 2016). Such evidence of time-transgressive The EBLF biome and climate variation trends during the mid- to late Holocene indicated by proxy records showed a pattern of temperature decline or unstable fluctuations, conflicting with modeled indications of sustained warming (Fig. 9a). This contradiction between the reconstructed cooling (or unstable

variation) and simulated progressive warming has been attributed to biases in the seasonality of the proxy reconstruction and climate sensitivity of models (Liu et al., 2015). Moreover, we found that the pollen assemblages indicating cooler conditions in the late Holocene were complex and differed from those from the last glacial period, as the evergreen forest components were not simply replaced by the deciduous components. Instead, grassland and secondary plant elements such as Poaceae, *Pinus*, and *Alnus* gradually increased. Some studies suggest that there was a decline in effective moisture in southern Asia resulted from the weakened summer monsoon and decreased precipitation since the middle Holocene (Li et al., 2020). In the meanwhile, the mean El Niño Southern Oscillation (ENSO) amplitude significantly increased (Clement et al., 2000), leading to frequent floods and droughts in China. Further, numerous proxy studies have indicated that a major loss of plant biodiversity, spread of rice cultivation and increasing frequency of fires in southern China occurred 2000-3000 years ago (Kaplan et al., 2011; Ma et al., 2020; Xu et al., 2021). Therefore, we suggest that combinations of factors, such as the weakening Asian summer monsoon, reduced precipitation and effective moisture, increased amplitude of ENSO events and associated changes in the western Pacific subtropical high, as well as fire frequencies associated with anthropogenic disturbances, may have affected the regional climate and thus EBLF/DBLF forest transformation from the mid- to late Holocene.

4. Conclusion

Although the EBLF components began to increase in low latitude regions during the deglaciation, biome change from deciduous to evergreen forest in the southern subtropical zone did not begin until

11.3 ka, after the Younger Dryas when regional annual and winter temperatures reached the zonal average thresholds of ~16.7°C and ~8.0°C, respectively. These values are highly consistent with the simulated results for current EBLF distribution. Both modeled and proxy data are consistent with the early Holocene being a key period when climatic thresholds (particularly winter and annual temperatures) approached then exceeded bioclimatic constraints for EBLF expansion. The EBLF biome recolonized the entire subtropical landscape including northern and mountainous areas during 8-5 ka, when regional air temperature (Tann) was higher than 15°C, indicating a warmest climate interval in accordance with the age of HTM commonly defined by multi-proxy records in China. Our integrated data indicate a time transgressive pattern that an earlier forest replacement at sites in low latitude regions as compared to sites located further north or at higher elevation in the subtropical zone of east China. This study highlights the greater importance of postglacial warming than rainfall changes for the EBLF recolonization across southeast China. However, the environment factors causing forest changes in the latter half of the Holocene were more complex. The sensitivity of forest responses to complex seasonal and abrupt climate changes (such as ENSO events), as well as increasing human activities during the late Holocene, may lead to the pollen-based climate reconstruction different from the model results. Our study provides new quantitative information regarding past biome and climate changes, as well as thresholds for forest transformation, that enhance understanding of long-term vegetation dynamics in the ecologically sensitive region between temperate and tropical bioclimatic zones. The observed amplitude of subtropical ecosystem changes during the postglacial warming may also serve as an analog for projections of forest responses to the increasing greenhouse conditions expected under future climate scenarios.

Acknowledgments

Funding: This work was financially supported by the National Key R&D Program of China (grant numbers 2022YFF0801500; 2016YFA0600500), the National Natural Science Foundation of China (NSFC) (grant numbers 42072205, 42077414, 41472143, 41630753, 41230101) and the China Postdoctoral Science Foundation (grant number 2021M703659), and is a contribution to the Belmont Forum funded project VULPES (Project ID: ANR-15-MASC-0003).

CRediT authorship contribution statement

Zhuo Zheng: Conceptualization, Investigation, Methodology, Formal analysis, Writing – original draft, Writing – review & editing, Funding acquisition. **Cong Chen:** Investigation, Methodology, Data curation, Formal analysis, Writing – review & editing, Funding acquisition. **Kangyou Huang:** Conceptualization, Investigation, Methodology, Data curation, Writing – review & editing, Funding acquisition. **Xiao Zhang:** Investigation, Methodology, Data curation, Software, Formal analysis, Writing – review & editing. **Peter Kershaw:** Conceptualization, Writing – review & editing. **Jun Cheng:** Methodology, Validation, Writing – review & editing**. Jie Li:** Investigation, Methodology. **Yuanfu Yue:** Investigation, Methodology. **Qiuchi Wan:** Investigation, Methodology. **Yaze Zhang:** Investigation, Methodology. **Ting Ma:** Investigation, Methodology**. Mengyuan Wang:** Investigation, Methodology**. Xiayun Xiao:** Methodology, Writing – review & editing. **Rachid Cheddadi:** Investigation, Writing – review & editing.

Declaration of Competing Interest

The authors declare that they have no known competing financial interests or personal relationships that could have appeared to influence the work reported in this paper.

Data availability

Data of biome and climate reconstructions can be found in the Supplementary data. Modern pollen dataset from EAPD for climate reconstruction is shared at https://doi.org/10.5281/zenodo.6918393.

References

An, Z.S., Porter, S.C., Kutzbach, J.E., Wu, X.H., Wang, S.M., Liu, X.D., Li, X.Q., Zhou, W.J., 2000. Asynchronous Holocene optimum of the East Asian monsoon. Quat. Sci. Rev. 19, 743–762. https://doi.org/10.1016/S0277-3791(99)00031-1.

Baggenstos, D., Haberli, M., Schmitt, J., Shackleton, S.A., Birner, B., Severinghaus, J.P., Kellerhals, T., Fischer, H., 2019. Earth's radiative imbalance from the Last Glacial Maximum to the present. Proc. Natl Acad. Sci. U.S.A. 116, 14881–14886. https://doi.org/10.1073/pnas.1905447116.

Bai, K.D., Jiang, D.B., Cao, K.F., Wan, X.C., Liao, D.B., 2010. Photosynthetic response to seasonal temperature changes in evergreen and deciduous broad-leaved trees in montane forests of Ailao Mountain and Mao'er Mountain. Acta Ecol. Sin. 30, 905–913.

Cao, X.Y., Ni, J., Herzschuh, U., Wang, Y.B., Zhao, Y., 2013. A late Quaternary pollen dataset from

612 eastern continental Asia for vegetation and climate reconstructions: Set up and evaluation. Rev.
613 Palaeobot. Palynology. 194, 21–37. https://doi.org/10.1016/j.revpalbo.2013.02.003.

614 Chen, Y., Ni, J., Herzschuh, U., 2010. Quantifying modern biomes based on surface pollen data in
615 China. Glob. Planet. Change. 74(3–4), 114–131. https://doi.org/10.1016/j.gloplacha.2010.09.002.

616 Cheng, Y., Liu, H., Wang, H.Y., Hao, Q., 2018. Differentiated climate-driven Holocene biome migra-
617 tion in western and eastern China as mediated by topography. Earth-Sci. Rev. 182, 174–185.
618 https://doi.org/10.1016/j.earscirev.2018.05.006.

619 Cheng, H., Zhang, H.W., Spoetl, C., Baker, J., Sinha, A., Li, H.Y., Bartolome, M., Moreno, A., Katha-
620 yat, G., Zhao, J.Y., Dong, X.Y., Li, Y.W., Ning, Y.F., Jia, X., Zong, B.Y., Brahim, Y.A., Perez-Mejias,
621 C., Cai, Y.J., Novello, V.F., Cruz, F.W., Severinghaus, J.P., An, Z.S., Edwards, R.L., 2020. Timing
622 and structure of the Younger Dryas event and its underlying climate dynamics. Proc. Natl Acad. Sci.
623 U.S.A. 117(38), 23408–23417. https://doi.org/10.1073/pnas.2007869117.

624 Cheng, J., Wu, H.B., Liu, Z.Y., Gu, P., Wang, J.J., Zhao, C., Li, Q., Chen, H.S., Lu, H.Y., Hu, H.B.,
625 Gao, Y., Yu, M., Song, Y.M., 2021. Vegetation feedback causes delayed ecosystem response to East
626 Asian summer monsoon rainfall during the Holocene. Nat. Commun. 12(1), 1843.
627 https://doi.org/10.1038%2Fs41467-021-22087-2.

628 Clement, A.C., Seager, R., Cane, M.A., 2000. Suppression of El Nino during the mid-Holocene by
629 changes in the Earth's orbit. Paleoceanogr. Paleoclimatology. 15(6), 731–737.
630 https://doi.org/10.1029/1999pa000466.

631 Dykoski, C.A., Edwards, R.L., Cheng, H., Yuan, D., Cai, Y., Zhang, M., Lin, Y., Qing, J., An, Z.,

632 Revenaugh, J., 2005. A high-resolution, absolute-dated Holocene and deglacial Asian monsoon rec-
633 ord from Dongge cave, China. Earth Planet. Sci. Lett. 233, 71–86.
634 https://doi.org/10.1016/j.epsl.2005.01.036.

635 DiNezio, P.N., Tierney, J.E., 2013. The effect of sea level on glacial Indo-Pacific climate. Nat. Geosci.
636 6(6), 485-491. https://doi.org/10.1038/ngeo1823.

637 Fang, J.Y., Yoda, K., 1991. Climate and vegetation in China V. Effect of climatic factors on the upper
638 limit of distribution of evergreen broadleaf forest. Ecol. Res. 6, 113–125.
639 https://doi.org/10.1007/BF02353874.

640 Fang, J.Y., Song, Y.C., Liu, H.Y., Piao, S.L., 2002. Vegetation-climate relationship and its application
641 in the division of vegetation zone in China. J. Integr. Plant Biol. 44(9), 1105–1122.

642 Fang, J.Y., Wang, Z.H., Tang, Z.Y., Fang, J.Y., Wang, Z.H., Tang, Z.Y., 2011. Atlas of Woody Plants in
643 China: Distribution and Climate. Springer & Higher Education Press, Berlin.

644 Faegri, K., Iversen, J., 1989. Textbook of Pollen Analysis. John, W. & Sons, Chichester.

645 Gao, Y., Xiong, K.N., Quan, M.Y., Song, B., Peng, H.J., Peng, H.R., Shen, W.D., Bao, K.S., 2019.
646 Holocene climate dynamics derived from pollen record of Jiulongchi wetland in Fanjing mountain,
647 southwest China. Quat. Int. 513, 1-7. https://doi.org/10.1016/j.quaint.2019.01.009.

648 Gotanda, K., Nakagawa, T., Tarasov, P., Kitagawa, J., Inoue, Y., Yasuda, Y., 2002. Biome classification
649 from Japanese pollen data: Application to modern-day and Late Quaternary samples. Quat. Sci.
650 Rev. 21(4–6), 647–657. https://doi.org/10.1016/S0277-3791(01)00046-4.

651 Han, A.Y., Zeng L.F., Huang, K.Y., Liao, W.B., Zheng, Z., Chen C., 2016. Holocene climate records
652 from a mountain wetland in Luoxiao ranges. Trop. Geogr. 36(3), 477–485.
653 https://10.13284/j.cnki.rddl.002855.

654 Harrison, S.P., Yu, G., Takahara, H., Prentice, I.C., 2001. Palaeovegetation diversity of temperate plants
655 in East Asia. Nature. 413(6852), 129–130. https://doi.org/10.1038/35093166.

656 He, J., Zhao, M.X., Li, L., Wang, H., Wang, P.X., 2008. Biomarker evidence of relatively stable com-
657 munity structure in the northern South China Sea during the Last Glacial and Holocene. Terr. Atmos.
658 Ocean Sci. 19, 377–387. https://doi.org/10.3319/TAO.2008.19.4.377(IMAGES).

659 Hijmans, R.J., Cameron, S.E., Parra, J.L., Jones, P.G., Jarvis, A., 2005. Very high resolution interpo-
660 lated climate surfaces for global land areas. Int. J. Climatol. 25(15), 1965–1978.
661 https://doi.org/10.1002/joc.1276.

662 Hu, C.H., Liu, J., Cai, S.Q., Li, Z.Q., 2014. Climate boundaries in vertical forest vegetation zonation
663 of subtropical east Chinese mountains-a case of the southwest mountainous areas in Zhejiang. Re-
664 sour. Environ. Yangtze Basin. 23(S1), 143–148.

665 Jiang, D.B., Lang, X.M., Tian, Z.P., Guo, D.L., 2011. Last glacial maximum climate over China from
666 PMIP simulations. Palaeogeogr. Palaeoclimatol. Palaeoecol. 309(3-4), 347–357.
667 https://doi.org/10.1016/j.palaeo.2011.07.003.

668 Jiang, W.Y., Leroy, S.A.G., Yang, S.L., Zhang, EL., Wang, L., Yang, X.X., Rioual, P., 2019. Synchro-
669 nous strengthening of the Indian and East Asian Monsoons in response to global warming since the
670 last deglaciation. Geophys. Res. Lett. 46(7), 3944–3952. https://doi.org/10.1029/2019gl082084.

671 Ju, L.X, Wang, H.J., Jiang, D.B., 2007. Simulation of the Last Glacial Maximum climate over East
672 Asia with a regional climate model nested in a general circulation model. Palaeogeogr. Palaeocli-
673 matol. Palaeoecol. 248(3-4), 376–390. https://doi.org/10.1016/j.palaeo.2006.12.012.

674 Juggins, S., Birks, H.J.B., 2012. Quantitative Environmental Reconstructions from Biological Data,
675 in: Birks, H.J.B., Lotter, A.F., Juggins, S., Smol, J.P. (Eds), Tracking Environmental Change Using
676 Lake Sediments. Developments in Paleoenvironmental Research, vol 5. Springer., Dordrecht, pp.
677 431–494.

678 Juggins, S., Telford, R.J., 2012. Exploratory Data Analysis and Data Display, in: Birks, H.J.B., Lotter,
679 A.F., Juggins, S., Smol, J.P. (Eds), Tracking Environmental Change Using Lake Sediments. Devel-
680 opments in Paleoenvironmental Research, vol 5. Springer., Dordrecht, pp. 123–141.

681 Juggins, S., 2017. Rioja: Analysis of Quaternary Science Data. R package version 0.9-21. http://cran.r-
682 project.org/package=rioja (accessed 13 May 2018).

683 Kageyama, M., Braconnot, P., Bopp, L., Caubel, A., Foujols, M.A., Guilyardi, E., Khodri, M., Lloyd,
684 J., Lombard, F., Mariotti, V., Marti, O., Roy, T., Woillez, M.N., 2013. Mid-Holocene and Last Gla-
685 cial Maximum climate simulations with the IPSL model-part I: Comparing IPSL_CM5A to
686 IPSL_CM4. Clim. Dyn. 40, 2447–2468. https://doi.org/10.1007/s00382-012-1488-8.

687 Kaplan, J.O., Krumhardt, K.M., Ellis, E.C., Ruddiman, W.F., Lemmen, C., Goldewijk, K.K., 2011.
688 Holocene carbon emissions as a result of anthropogenic land cover change. The Holocene. 21(5),
689 775–791. https://doi.org/10.1177/0959683610386983.

690 Lambeck, K., Rouby, H., Purcell, A., Sun, Y.Y., Sambridge, M., 2014. Sea level and global ice volumes

691 from the Last Glacial Maximum to the Holocene. Proc. Natl Acad. Sci. U.S.A. 111(43), 15296–
692 15303. https://doi.org/10.1073/pnas.1411762111.

693 Lee, C.Y., Liew, P.M., 2010. Late Quaternary vegetation and climate changes inferred from a pollen
694 record of Dongyuan Lake in southern Taiwan. Palaeogeogr. Palaeoclimatol. Palaeoecol. 287(1–4),
695 58–66. https://doi.org/10.1016/j.palaeo.2010.01.015.

696 Li, J., Zheng, Z., Huang, K.Y., Yang, S.X., Chase, B., Valsecchi, V., Carré, M., Cheddadi, R., 2013.
697 Vegetation changes during the past 40,000 years in Central China from a long fossil record. Quat.
698 Int. 310, 221–226. https://doi.org/10.1016/j.quaint.2012.01.009.

699 Li, Q., Wu, H.B., Yu, Y.Y., Sun, A.Z., Luo, Y.L., 2019. Large-scale vegetation history in China and its
700 response to climate change since the Last Glacial Maximum. Quat. Int. 500, 108–119.
701 https://doi.org/10.1016/j.quaint.2018.11.016.

702 Li, Y., Zhang, Y., Zhang, X., Ye, W., Xu, L., Han, Q., Li, Y., Liu, H., Peng, S., 2020. A continuous
703 simulation of Holocene effective moisture change represented by variability of virtual lake level in
704 East and Central Asia. Sci. China Earth Sci. 63, 1161–1175. https://doi.org/10.1007/s11430-019-
705 9576-x

706 Liew, P.-M., Huang, S.Y., Kuo, C.M., 2006. Pollen stratigraphy, vegetation and environment of the last
707 glacial and Holocene–A record from Toushe Basin, central Taiwan. Quat. Int. 147, 16–33.
708 https://doi.org/10.1016/j.quaint.2005.09.003

709 Liu, Y.L., Guo, R.Q., Sun, S.C., 2010. Variations in the vertical vegetation zonation of subtropical
710 Chinese mountains: The importance of climatic seasonality. Acta Bot. Sin. 30(14), 3912–3922.

711 Liu, Z., Otto-Bliesner, B.L., He, F., Brady, E.C., Tomas, R., Clark, P.U., Carlson, A.E., Lynch-Stieglitz,
712 J., Curry, W., Brook, E., Erickson, D., Jacob, R., Kutzbach, J., Cheng, J., 2009. Transient simulation
713 of last deglaciation with a new mechanism for Bølling-Allerød warming. Science. 325(5938), 310–
714 314. https://doi.org/10.1126/science.1171041.

715 Liu, Z.Y., Carlson, A.E., He, F., Brady, E.C., Otto-Bliesner, B.L., Briegleb, B.P., Wehrenberg, M.,
716 Clark, P.U., Wu, S., Cheng, J., Zhang, J.X., Noone, D., Zhu, J., 2012. Younger Dryas cooling and
717 the Greenland climate response to CO_2. Proc. Natl Acad. Sci. U.S.A. 109(28), 11101–11104.
718 https://doi.org/10.1073/pnas.1202183109.

719 Liu, Z.Y., Zhu, J., Rosenthal, Y., Zhang, X., Otto-Bliesner, B.L., Timmermann, A., Smith, R.S.,
720 Lohmann, G., Zheng, W.P., Timm, O.E., 2014. The Holocene temperature conundrum. Proc. Natl
721 Acad. Sci. U.S.A. 111(34), E3501-E3505. https://doi.org/10.1073/pnas.1407229111.

722 Ma, T., Tarasov, P.E., Zheng, Z., Han, A.Y., Huang, K.Y., 2016. Pollen- and charcoal-based evidence
723 for climatic and human impact on vegetation in the northern edge of Wuyi Mountains, China, during
724 the last 8200 years. The Holocene 26(10), 1616–1626.
725 https://doi.org/10.1073/10.1177/0959683616641744.

726 Ma, T., Zheng, Z., Man, M.L., Dong, Y.X., Li, J., Huang, K.Y., 2018. Holocene fire and forest histories
727 in relation to climate change and agriculture development in southeastern China. Quat. Int. 488, 30–
728 40. https://doi.org/10.1016/j.quaint.2017.07.035.

729 Ma, T., Rolett, B.V., Zheng, Z., Zong, Y.Q., 2020. Holocene coastal evolution preceded the expansion
730 of paddy field rice farming. Proc. Natl Acad. Sci. U.S.A. 117(39), 24138–24143.

https://doi.org/10.1073/pnas.1919217117.

Ni, J., Cao, X.Y., Jeltsch, F., Herzschuh, U., 2014. Biome distribution over the last 22,000yr in China. Palaeogeogr. Palaeoclimatol. Palaeoecol. 409, 33–47. https://doi.org/10.1016/j.palaeo.2014.04.023.

Parnell, A.C., Haslett, J., Allen, J.R.M., Buck, C.E., Huntley, B., 2008. A flexible approach to assessing synchroneity of past events using Bayesian reconstructions of sedimentation history. Quat. Sci. Rev. 27, 1872–1885. https://doi.org/10.1016/j.quascirev.2008.07.009

Peterse, F., van der Meer, J., Schouten, S., Weijers, J.W.H., Fierer, N., Jackson, R.B., Kim, J.H., Damste, J.S.S., 2012. Revised calibration of the MBT-CBT paleotemperature proxy based on branched tetraether membrane lipids in surface soils. Geochem. Cosmochim. Acta 96, 215-229. https://doi.org/10.1016/j.gca.2012.08.011.

Peng, H., Zheng, Z., Zheng, Y.W., Huang, K.Y., Wei, J.H., 2015. Holocene vegetarion changes and human activities revealed by a peat sediment core in Gaoyao, Zhaoqing. Quat. Sci. 35(3), 743–754. https://doi.org/10.11928/j.issn.1001-7410.20115.03.24.

Penny, D., 2001. A 40,000 year palynological record from north-east Thailand: Implications for biogeography and palaeo-environmental reconstruction. Palaeogeogr. Palaeoclimatol. Palaeoecol. 171(3-4), 97–128. https://doi.org/10.1016/s0031-0182(01)00242-5.

Reimer, P.J., Bard, E., Bayliss, A., Beck, J.W., Blackwell, P.G., Ramsey, C.B., Buck, C.E., Cheng, H., Edwards, R.L., Friedrich, M., Grootes, P.M., Guilderson, T.P., Haflidason, H., Hajdas, I., Hatte, C., Heaton, T.J., Hoffmann, D.L., Hogg, A.G., Hughen, K.A., Kaiser, K.F., Kromer, B., Manning, S.W., Niu, M., Reimer, R.W., Richards, D.A., Scott, E.M., Southon, J.R., Staff, R.A., Turney, C.S.M., van

751 der Plicht, J., 2013. Intcal13 and Maeinre13 radiocarbon age calibration curves 0–50,000 years cal
752 BP. Radiocarbon 55(4), 1869–1887. https://doi.org/10.2458/azu_js_rc.55.16947.

753 Reimi, M.A., Marcantonio, F., 2016. Constraints on the magnitude of the deglacial migration of the
754 ITCZ in the Central Equatorial Pacific Ocean. Earth Planet. Sci. Lett. 453, 1–8.
755 https://doi.org/10.1016/j.epsl.2016.07.058.

756 Ren W., Yi, G., 2019. Characteristics of time-transgressive Holocene Optimum in the East Asian mon-
757 soon region. Earth Sci. Res. J. 23: 259-263. https://doi.org/10.15446/esrj.v23n3.72188

758 Schouten, S., Hopmans, E.C., Damste, J.S.S., 2013. The organic geochemistry of glycerol dialkyl
759 glycerol tetraether lipids: a review. Org. Geochem. 54, 19-61. https://doi.org/10.1016/j.orggeo-
760 chem.2012.09.006.

761 Sheng, M., Wang, X.S., Zhang, S.Q., Chu, G.Q., Su, Y.L., Yang, Z.Y., 2017. A 20,000-year high-reso-
762 lution pollen record from Huguangyan Maar Lake in tropical-subtropical South China. Palaeogeogr.
763 Palaeoclimatol. Palaeoecol. 472, 83–92. https://doi.org/10.1016/j.palaeo.2017.01.038.

764 Shi, Y.F., Kong, Z.Z., Wang, S.M., Tang, L.Y., Wang, F.B., Yao, T.D., Zhao, X.T., Zhang, P.Y., Shi,
765 S.H., 1993. Mid-Holocene climates and environments in China. Glob. Planet. Change. 7(1–3), 219–
766 233. https://doi.org/10.1016/0921-8181(93)90052-P.

767 Song, Y.C., 1999. Perspective of the vegetation zonation of forest region in Eastern China. Acta Bot.
768 Sin. 41(5), 541–552. https://doi.org/10.1016/S0168-9452(99)00028-X.

769 Song, K., Da, L.J., 2016. Evergreen-deciduous broad-leaved forest ecotone in eastern China: Retro-
770 spect and new perspectives, in: Box, E.O. (Eds), Vegetation Structure and Function at Multiple
771 Spatial, Temporal and Conceptual Scales. Geotany Studies, Springer., Cham., pp. 129–147.

772 Tian, F., Cao, X.Y., Dallmeyer, A., Ni, J., Zhao, Y., Wang, Y.B., Herzschuh, U., 2016. Quantitative
773 woody cover reconstructions from eastern continental Asia of the last 22 kyr reveal strong regional
774 peculiarities. Quat. Sci. Rev. 137, 33–44. https://doi.org/10.1016/j.quascirev.2016.02.001.

775 Tian, Z.P., Jiang, D.B., 2016. Revisiting last glacial maximum climate over China and East Asian mon-
776 soon using PMIP3 simulations. Palaeogeogr. Palaeoclimatol. Palaeoecol. 453, 115–126.
777 https://doi.org/10.1016/j.palaeo.2016.04.020.

778 Wang, Y.J., Cheng, H., Edwards, R.L., An, Z.S., Wu, J.Y., Shen, C.C., Dorale, J.A., 2001. A high-
779 resolution absolute-dated late Pleistocene monsoon record from Hulu Cave, China. Science.
780 294(5550), 2345–2348. https://doi.org/10.1126/science.1064618.

781 Wang, M.Y., Zheng, Z., Man, M.L., Hu, J.F., Gao, Q.Z., 2017. Branched GDGT-based paleotempera-
782 ture reconstruction of the last 30, 000 years in humid monsoon region of Southeast China. Chem.
783 Geol. 463, 94–102. https://doi.org/10.1016/j.chemgeo.2017.05.014.

784 Weijers, J.W.H., Schouten, S., van den Donker, J.C., Hopmans, E.C., Damsté, J.S.S., 2007. Environ-
785 mental controls on bacterial tetraether membrane lipid distribution in soils. Geochim. Cosmochim.
786 Acta 71, 703–713. https://doi.org/10.1016/j.gca.2006.10.003.

787 Wu, Z.Y., 1980. Vegetation of China. Science Press, Beijing.

788 Xiao, J.Y., Lü, H.B., Zhou, W.J., Zhao, Z.J., Hao, R.H., 2007. Evolution of vegetation and climate
789 since the last glacial maximum recorded at Dahu peat site, South China. Sci. China Earth Sci. 50,
790 1209–1217. https://doi.org/10.1007/s11430-007-0068-y.

791 Xiao, X.Y., Haberle, S.G., Shen, J., Yang, X.D., Han, Y., Zhang, E.L., Wang, S.M., 2014. Latest Pleis-
792 tocene and Holocene vegetation and climate history inferred from an alpine lacustrine record, north-
793 western Yunnan Province, southwestern China. Quat. Sci. Rev. 86, 35–48.
794 https://doi.org/10.1016/j.quascirev.2013.12.023.

795 Xu, Y.Z., Franklin, S.B., Wang, Q.G., Shi, Z., Luo, Y.Q., Lu, Z.J., Zhang, J.X., Qiao, X.J., Jiang,
796 M.X., 2015. Topographic and biotic factors determine forest biomass spatial distribution in a sub-
797 tropical mountain moist forest. For. Ecol. & Manage. 357, 95–103.
798 https://doi.org/10.1016/j.foreco.2015.08.010.

799 Xu, X., Li, F., Lin, Z.D., Song, X., 2021. Holocene fire history in China: Responses to climate
800 change and human activities. Sci. Total Environ. 753, 142019. https://doi.org/10.1016/j.sci-
801 totenv.2020.142019.

802 Yu, G., Chen, X., Ni, J., Cheddadi, R., Guiot, J., Han, H., Harrison, S.P., Huang, C., Ke, M., Kong, Z.,
803 Li, S., Li, W., Liew, P., Liu, G., Liu, J., Liu, Q., Liu, K.B., Prentice, I.C., Qui, W., Ren, G., Song,
804 C., Sugita, S., Sun, X., Tang, L., Van Campo, E., Xia, Y., Xu, Q., Yan, S., Yang, X., Zhao, J., Zheng,
805 Z., 2000. Palaeovegetation of China: a pollen data-based synthesis for the mid-Holocene and last
806 glacial maximum. J. Biogeogr. 27(3), 635–664. https://doi.org/10.1046/j.1365-2699.2000.00431.x.

807 Yue, Y.F., Zheng, Z., Huang, K.Y., Chevalier, M., Chase, B.M., Carre, M., Ledru, M.P., Cheddadi, R.,

2012. A continuous record of vegetation and climate change over the past 50,000 years in the Fujian Province of eastern subtropical China. Palaeogeogr. Palaeoclimatol. Palaeoecol. 365, 115–123. https://doi.org/10.1016/j.palaeo.2012.09.018.

Zhang, X., Zheng, Z., Huang, K.Y., Yang, X.Q., Tian, L.P., 2020. Sensitivity of altitudinal vegetation in southwest China to changes in the Indian summer monsoon during the past 68000 years. Quat. Sci. Rev. 239, 106359. https://doi.org/10.1016/j.quascirev.2020.106359.

Zhao, Y., Yu, Z.C., Chen, F.H., Zhang, J.W., Yang, B., 2009. Vegetation response to Holocene climate change in monsoon-influenced region of China. Earth Sci. Rev. 97(1), 242–256. https://doi.org/10.1016/j.earscirev.2009.10.007.

[dataset] Zheng, Z., Huang, K.Y., 2022. Modern pollen data from the East Asian Pollen Database (EAPD): pollen, vegetation and climate relationship. https://doi.org/10.5281/zenodo.6918393.

Zheng, Z. Wang, J.H., Wang, B. Liu, C.L., Zou, H.P., Zhang, H., Deng, Y., Bai, Y., 2003. High-resolution records of Holocene from the Shuangchi Maar Lake in Hainan Island. Chin. Sci. Bul., 48(5), 497–502. http://doi.org/ 10.3321/j.issn:0023-074X.2003.03.017

Zheng, Z., Wei, J.H., Huang, K.Y., Xu, Q.H., Lu, H.Y., Tarasov, P., Luo, C.X., Beaudouin, C., Deng, Y., Pan, A., Zheng, Y.W., Luo, Y.L., Nakagawa, T., Li, C.H., Yang, S.X., Peng, H.H., Cheddadi, R., 2014. East Asian pollen database: modern pollen distribution and its quantitative relationship with vegetation and climate. J. Biogeogr. 41(10), 1819–1832. https://doi.org/10.1111/jbi.12361.

Zheng, Z., Zhang, X., Man, M.L., Wei, J.H., Huang, K.Y., 2016. Review and data integration of pollen-based quantitative paleoclimate reconstruction studies in China and adjacent areas. Quat. Sci. 36(3),

503–519. https://doi.org/10.1039/D1MA00229E.

Zhong, W., Cao, J.Y., Xue, J.B., Ouyang, J., 2015. Last deglacial and Holocene vegetation evolution and climate variability in the subalpine western Nanling Mountains in South China. The Holocene 25(8), 1330–1340. https://doi.org/10.1177/095968361558.

Zhou, X., Sun, L.G., Zhan, T., Huang, W., Zhou, X.Y., Hao, Q.Z., Wang, Y.H., He, X.Q., Zhao, C., Zhang, J., Qiao, Y.S., Ge, J.Y., Yan, P., Yan, Q., Shao, D., Chu, Z.D., Yang, W.Q., Smol, J.P., 2016. Time-transgressive onset of the Holocene optimum in the East Asian monsoon region. Earth Planet. Sci. Lett. 456, 39–46. https://doi.org/10.1016/j.epsl.2016.09.052.

Zhou, X., Zhan, T., Tu, L., Smol, J.P., Jiang, S., Liu, X., Xu, C., Guo, Z., 2022. Monthly insolation linked to the time-transgressive nature of the Holocene East Asian monsoon precipitation maximum. Geology, 50, 331–335. https://doi.org/10.1130/G49550.1